UNIVERSITY OF CALIFORNIA SAN DIEGO

Study of Human Retinal Ganglion Cell Development and Direct Conversion

A thesis submitted in partial satisfaction of the requirements
for the degree of Master of Science

in

Biology

by

Mona Pari Roshan

Committee in charge:

Professor Karl Wahlin, Chair
Professor Alisa Huffaker, Co-Chair
Professor James Cooke

2021

The thesis of Mona Roshan is approved, and is acceptable in quality and Form for publication on microfilm and electronically.

University of California San Diego

2021

DEDICATIONS

Dedicated to my family and friends for all their love and support throughout my research endeavors.

TABLE OF CONTENTS

LIST OF FIGURES

LIST OF TABLES

ABBREVIATIONS

3G-TRE	TET response element
APC	Adenomatosis polyposis coli
ATOH7	Atonal 7
Ascl1	Achaete-scute homolog 1
Ascl1a	Achaete-scute homolog 1a
BDNF	Brain-derived Neurotrophic Factor
BMP	Bone Morphogenic Protein
BMP7	Bone Morphogenic Protein 7
BRN3B / POU4F2	Brain-3B
CK1α	Casein kinase 1α
CNTF	Ciliary Neurotrophic Factor
Cbh	Chicken beta-actin hybrid
DMSO	Dimethyl sulfoxide
Dox/Doxy	Doxycycline
DM	Differentiation Medium
ECM	Extracellular matrix
FGF	Fibroblast Growth Factors
FZD	Frizzled receptor
GSK3	Glycogen synthase kinase 3
Gli	Glioma-associated oncogene homolog
HDR	Homology directed repair
IGF	Insulin-like Growth factors
INL	Inner nuclear layer
IPL	Inner plexiform layer
ISL1	Islet-1
LATS1/2	Large Tumor Suppressor Kinase ½
LB	Lysogeny broth
LRP5/6	Low-density lipoprotein receptor-related protein 5/6
MAP4K	Mitogen-Activated Protein Kinase Kinase Kinase Kinase
MG	Müller glia
MST1/2	Mammalian STE20-Like Protein Kinase 1/2
NAIB	NEUROG2, ATOH7, ISL1, and BRN3B (POU4F2)
NAIP1	NEUROG2, ATOH7, ISL1, and BRN3B (POU4F1)
NEB	New England Biolabs
NGN2 / NEUROG2	Neurogenin-2
NIM	Neural Induction Medium
ONL	Outer nuclear layer
OPL	Outer plexiform layer
PAM	Protospacer adjacent motif
PCR	Polymerase chain reaction
PP2A	Protein phosphatase 2A
PSC	Pluripotent stem cell
Ptch1	Patched

R-Smads	Receptor-regulated Smads
RGC	Retinal ganglion cell
RPE	Retinal pigment epithelium
Shh	Sonic hedgehog
Smo	Smoothened
Sox	Sry-related high mobility box
SOX2	Sex determining region Y-box 2
TAZ	Transcriptional Co-Activator with PDZ-Binding Motif
TEAD 1-4	TEA Domain transcription factors
TET	Tetracycline
TGF- β	Transforming Growth Factor β
Tm	primer melting temperature
YAP	Yes Associated Protein
cDNA	Complementary DNA
gDNA	Genomic DNA
gRNA	Guide RNA
iPSC	Induced pluripotent stem cell
rtTA	Reverse tetracycline trans-activating sequence

ACKNOWLEDGMENTS

I would like to extend my deepest gratitude to Dr. Karl Wahlin for the opportunity to do research in his lab and his continued support as my principal investigator and the chair of my thesis committee. His mentorship, guidance and expertise were invaluable throughout my time working in the lab. His insightful feedback and scholarly advice pushed me to sharpen my critical thinking and become a better scientist. It was a great privilege and honor to conduct research under his guidance.

I also wish to thank the members of the Wahlin Lab, past and present, for their friendship and unwavering support. I am so appreciative of all their help and for creating a collaborative working environment.

ABSTRACT OF THE THESIS

Directional Outgrowth of Retinal Ganglion Cells

by

Mona Pari Roshan

Master of Science in Biology

University of California San Diego, 2021

Professor Karl Wahlin, Chair

Professor Alisa Huffaker, Co-Chair

The loss of retinal ganglion cells (RGCs) causes irreversible vision loss in glaucoma and optic neuropathies. Some vertebrate species, such as zebrafish, possess a robust ability to regenerate parts of their body, including the retina through a process of endogenous regeneration. However, this ability is limited in mammals including humans. To understand endogenous regeneration and work towards restoring RGCs, we need to gain a better understanding of the developmental mechanisms leading to RGC formation. Our approach relies on the generation of RGC reporters that express fluorescent proteins coupled to the endogenous BRN3A and BRN3B

genes. By ectopically overexpressing four transcription factors (Neurogenin-2, Atonal homolog 7, Islet-1, and Brn3b) involved in RGC specification and differentiation, we seek to directly convert the human pluripotent stem cell reporters into RGCs. If the differentiated neurons become bonafide BRN3A/BRN3B expressing RGCs, this would represent an important first step in developing and improving novel therapeutic strategies for retinal diseases.

INTRODUCTION

Vision disorders and treatments

Optic neuropathies consist of a group of degenerative disorders, such as optic neuritis, neuromyelitis optica, and glaucoma, that target RGCs and thereby, lead to vision loss and blindness. Of the many optic neuropathies, glaucoma is the leading cause of irreversible blindness worldwide, affecting 70 million individuals globally (Weinreb et al., 2014). It is caused by the degeneration of RGCs and is often first detected by changes in the optic nerve head, where RGC axons leave the back of the eye and project towards the lateral geniculate nucleus, superior colliculus, suprachiasmatic nucleus and medial terminal nucleus. RGCs are neurons in the central nervous system that have their cell bodies in the inner retina and their axons in the optic nerve (Weinreb et al., 2014). They are essential for the transmission of visual information between the eye and brain (Fligor et al., 2018). The degeneration of these nerves leads to a phenomenon typical of glaucoma called cupping, in which the optic cup becomes larger than the disc, and eventual vision loss. The rise of intraocular pressure results in the progressive loss of RGCs (Weinreb et al., 2014). In addition, the deformation of the lamina cribrosa, consisting of connective tissue, glial cells and microvessels that support RGC axons, is the earliest structural change that results in the RGC loss (Kim et al., 2018). The architecture of the eye, including the optic nerve and the lamina cribrosa, is illustrated in **Figure 1**.

Although there are various therapeutics that can prevent or slow further ganglion cell damage, there is no definitive cure for glaucoma. Some of the therapeutics include purinergic ligands like P2X7 antagonists, K_{ATP} channel activators, gaseous messengers like nitric oxide, carbon monoxide, hydrogen sulfide, non-glucocorticoid steroidal compounds, neurotrophic factors, PI3K/AKT activators, histone deacetylase inhibitors, citicoline, dopaminergic and

serotonergic ligands, cannabinoids, and Rho Kinase (ROCK) inhibitors (Buculo et al., 2018). While not all forms of glaucoma are accompanied by increased pressure, many of these therapeutics serve to reduce the intraocular pressure in the eye. These therapeutics have been successful in treating glaucoma for many patients (Buculo et al., 2018). However, for many patients, these therapeutics do not work, and the pressure rises; this is when surgical intervention becomes necessary (Stefan et al., 2015).

Human eye development and retinogenesis

Mammalian eye development stems from the neural ectoderm, the surface ectoderm, and the periocular mesenchyme, three embryonic tissue sources (Heavner and Pevny, 2012). Following gastrulation, the eye primordium (the eye field) is formed within the medial anterior neural plate (Zaghloul et al., 2005). This eye field is the foundation for the neural-derived eye and expresses various transcription factors, such *Pax6*, *Rax*, *Six3*, and *Lhx2*, that are conserved throughout vertebrates (Zaghloul et al., 2005; Lee et al., 2006; Zuber et al., 2003). The area within the medial anterior neural plate that has high expression of these transcription factors is the eye field (Zuber et al., 2003). In addition to the eye, these transcription factors are also involved in forebrain development.

In humans, the morphogenetic processes leading to the development of the human eye are related to other structures of the central nervous system at the start of embryogenesis (Tamm et al., 2012). Both processes start toward the end of the third week of human embryonic development with the differentiation of the neural plate, which is characterized by the thickening of the ectoderm (Tamm et al., 2012). Neural plate induction is induced by the inhibition of Bone Morphogenic Protein (BMP) signaling. Wnts and Wnt inhibitors, insulin-like growth factors (IGF), and fibroblast growth factors (FGF) are also involved in this early process (Giger, 2018).

The neural plate then forms the neural groove, encompassing the entire length of the embryo. The neural groove's edges then thicken to develop the neural folds that move towards each other and eventually fuse to form the neural tube, the foundation of the brain and spinal cord (Tamm et al., 2012). Outgrowth of the neural tube then occurs to form the optic vesicles. The process leading up to the development of the optic vesicles is regulated by the Retina and Anterior Neural Fold Homeobox (RX/RAX) transcription factor (Fuhrmann et al., 2010). The rostral end of the neural tube becomes the forebrain and connections to the forebrain become the optic nerves (Tamm et al., 2012).

During the fifth week of embryogenesis, the growing optic vesicle makes direct contact with the ectoderm, which results in the thickening of the ectoderm, to form the lens placode (Tamm et al., 2012). Further development of the lens placode and the optic vesicle is mediated by diffusible signal molecules that specify cell fates and activate transcription factors, which bind to DNA and regulate transcription of eye related genes. Pax6 is a key transcription factor that regulates mammalian eye development (Gehring, 2002; Perrimon et al., 2012). Due to Pax6 signaling, the optic vesicle invaginates into a goblet shaped optic cup, while the lens placode invaginates and forms a pouch called the lens pit (Tamm et al., 2012). This lens pit becomes completely enclosed and becomes the lens vesicle, which develops into the lens. The inner layer of the optic cup differentiates into the neural retina, while the outer layer differentiates into the retinal pigment epithelium (RPE) (Eiraku et al., 2011). Neural retina differentiation is supported by tissue-autonomous factors. RPE differentiation involves interaction with neighboring issues through canonical Wnt signaling. Wnt receptor frizzled class receptor 7 (FZD7), Wnt ligand binding secreted frizzled-related protein 5 (SFRP5), and membrane frizzled-related protein (MFRP) which has a Wnt binding motif have been detected on the RPE (Burke, 2009). BMPs

regulate optic cup development. Also, the outpocketing of the neuroectodermal neural tubes transforms into the optic vesicles and later into the optic cup. Folds in the outer layer of the optic cup result in the epithelia of the ciliary body, which is a ring-shaped muscle that not only changes pupil size and lens shape when the eye focuses but also secrete aqueous humor in the adult eye (Tamm et al., 2012).

The neural crest consists of cells which have separated from the optic vesicle during its development (Tamm et al., 2012). They also come from the region in between the neural plate and adjacent non-neural ectoderm (Bronner & LeDouarin, 2012). During the formation of the optic cup and the lens vesicle in the fifth week of embryogenesis, these nearby mesenchymal cells surround those two structures. Due to their loose arrangement, a large fibrillary extracellular matrix is formed, a space that will later become the corneal stroma. Gradually, the mesenchymal cells proliferate and densify (Tamm et al., 2012). The mesenchymal cell layer next to the anterior lens epithelium flattens, forms continuous cell connections, and by the end of the eighth week of embryogenesis, differentiates into the corneal endothelium. Then, the anterior lens epithelium and the cornea detach from one another (Tamm et al., 2012). The division and proliferation of the anterior cells of the optic cup leads to the development of the iris and the ciliary body. In addition to those two structures, the sclera is formed by the mesenchymal cells originating from the neural crest.

Retinal development stems from the optic cup. The neuroretina contains the retinal neurons, of which the Müller cells come from its inner leaf and the retinal pigment epithelium come from its outer leaf (Tamm et al., 2012). Following the formation of the eye cup, the inner leaf of the optic cup proliferate and by the sixth week of embryogenesis, there are up to six neuronal progenitor, or neuroblast, cell nucleus layers (Tamm et al., 2012). During the seventh

week of embryogenesis, the outermost cell nucleus layer migrates towards the marginal layer to create the inner neuroblast layer, which will differentiate into the amacrine cells, retinal ganglion cells and lastly, the Müller cells (Tamm et al., 2012). Once the retinal ganglion cells are differentiated, their axons elongate into the optic papilla, forming the nerve fiber layer within the inner neuroblast layer (Spira & Hollenberg, 1973). Retinal ganglion cells continue to proliferate until the fourth month of embryogenesis. At that point, there are around four million axons in the optic nerve. However, up until the eighth month of embryogenesis and as the retina continues to differentiate, the number of retinal ganglion cells decrease due to apoptosis to around 1.1 million (Provis et al., 1985). The cones start to develop during the tenth week and elongate up to the seventeenth week. The rods start to develop later during the twenty second week (Spira & Hollenberg, 1973). **Figure 2** illustrates the steps of human eye development.

Many morphogens and growth factors are involved in eye development. The splitting of the eye field in addition to the proximo-distal patterning of the optic vesicles involve cyclops (IPD3) and sonic hedgehog (Shh) signaling (Adler & Canto-Soler, 2007). Sonic hedgehog, fibroblast growth factors, activin, BMP 7, and retinoic acid are also necessary for optic vesicle patterning. The invagination of the optic vesicle into an optic cup utilizes retinoic acid (RA) in particular. *Rald2* and *Rald3* are the genes that generate RA, which stimulates the ventral morphogenetic movements of the optic vesicle that starts the formation of the ventral optic cup. RA also closes the choroid fissure (Duester, 2009). When RA is synthesized, RA binds to the cellular RA-binding proteins, CRABP1/2, which results in a conformational change that allows both proteins to enter the nucleus. In the nucleus, RA binds to a non-steroid hormone receptor family that includes RARα/β/γ, and RXRα/β/γ. These receptors regulate genes necessary for eye development. They usually recruit transcriptional co-repressor complexes. However, when RA is

bound, a conformational change occurs in the receptors that results in their recruitment of transcriptional co-activator complexes instead. Thus, RA binding allows for the transcription of genes required for optic cup formation (Cvekl & Wang, 2010). Lastly, the antero-posterior and dorso-ventral patterning in the optic cup are regulated by nodal, FGFs, BMP, retinoic acid, Shh, follistatin, chordin, noggin, ventroptin, and DAN domain family members (Albert et al., 2003).

Retinal lamination and cell types

The retina, the innermost layer of the eye, converts light into neural signals that are sent to the brain, where visual perception occurs (Masland et al., 2012). The retina is characterized by the cells that compose its three layers of nerve cell bodies and two layers of synapses (Kolb, 2012). There are five main types of neuronal cells in the retina. These consist of ganglion cells, photoreceptors (rods and cones), horizontal cells, amacrine cells, and bipolar cells. There are three types of glial cells, including microglia, astrocytes, and Müller glia. The outer nuclear layer (ONL) of the retina is composed of the photoreceptors, which include the rods as well as the blue, red and green sensitive cones. Photoreceptors, in addition to the intrinsically photosensitive RGCs (ipRGCs), are the primary cells that convert light into signals that are eventually sent to the brain. Their axons elongate towards the outer plexiform layer (OPL), where synaptic triad is formed with bipolar and horizontal cells. Bipolar cells in turn synapse with RGCs in the inner plexiform layer (IPL) that send light signals towards the brain. Using lateral inhibition, amacrine and horizontal cells modulate these light signals to allow for a high degree of visual acuity (Masri, 2019). **Figure 3** illustrates the cell types of the retina.

RGCs have many different subtypes. Through single-cell RNA-sequencing in the mouse retina, RGCs were classified into more than forty different subtypes (Laboissonniere et al., 2019). Within hPSC-derived cultures, more than thirty different RGC subtypes have been

characterized and they vary in gene expression patterns, morphology, and functionality (Dhande et al., 2015). Light activates the RGC dendrites within the inner layers of the inner plexiform layer (IPL); this is the ON pathway. Those within the outer layers of the IPL are inhibited by light; this is the OFF pathway (Nelson et al., 1978).

Most RGC axons cross the midline at the optic chiasm and follow the contralateral optic tract towards the brain. Animal species with binocular vision also possess RGC axons that do not cross the midline, but rather follow the ipsilateral optic tract (Fabre et al., 2010). Contralateral RGCs are regulated by SoxC transcription factors, including Sox4, Sox11 and Sox12 (Kuwajima et al., 2017). Ipsilateral RGCs are found in the ventrotemporal (VT) part of the retina and highly express genes that are known to be expressed by retinal progenitor cells such as cyclin D2 (Fabre et al., 2010; Wang et al., 2016).

Based on their projection specificity, there are five main categories of RGCs, which include the midget cells, parasol cells, bistratified cells, ipRGCs, and other ganglion cells projecting to the superior colliculus for eye movements (Schiller, 1986). Most RGCs project to the lateral geniculate nucleus (LGN) in the dorsal thalamus (Sanes & Masland, 2015). A diagram of the LGN is shown in **Figure 4**. 80% of all RGCs, the midget cells project to the parvocellular layers of the LGN. They help with encoding high resolution vision and red/green color vision. 10% of all RGCs, the parasol cells project to the magnocellular layers of the LGN and are responsible for motion detection. 10% of all RGCs, the bistratified cells project to the koniocellular layers of the LGN and are involved in spatial resolution, color vision, conduction velocity, and contrast stimuli response. On the other hand, ipRGCs mainly project to the suprachiasmatic nucleus (SCN) and respond directly to light due to their expression of

melanopsin, a photopigment. Their main role is to regulate circadian rhythms (Sanes & Masland, 2015).

Transcription factor involvement in eye development

Pax6, Six3, Lhx2, and Rax are a set of transcription factors expressed in the early eye field. They are necessary for not only eye development but also forebrain development; thus, the upstream pathways for the development of the eye field are difficult to classify (Heavner et al., 2012). Sonic Hedgehog signaling regulates the expression of Pax6, which is a master regulator of eye development (Isenmann et al., 2003). Six3 is expressed before Pax6, as it is a transcription factor that activates Pax6 transcription. SOX2 is activated by BMP4 signaling and Pax6 is activated by BMP7 signaling (Heavner et al., 2012).

RGC development is regulated by multiple transcription factors, including Neurogenin-2 (NEUROG2), Atonal homolog 7 (ATOH7), Islet-1 (ISL1), Neurod-1 (NEUROD1), and Achaete-scute homolog 1 (ASCL1). These transcription factors influence differentiation, cell cycle exit and cell survival, overall regulating neurogenesis (Luo et al., 2019). BRN3A (POU4F1) and BRN3B (POU4F2) are other transcription factors that control the differentiation of retinal precursors into RGCs (Xiang et al., 2011). In mice, around 80% of RGC precursors express *Brn3a* and *Brn3b* (Pan et al., 2005). *Brn3a*- and *Brn3b*- expressing RGCs have varying dendritic stratification; the *Brn3a*-expressing RGCs stratify in the outer layer of the IPL. They both project to the same targets, except for the suprachiasmatic region and the intergeniculate leaflet (Badea et al., 2009).

The loss in expression of *Brn3a* and *Brn3a* has varying effects. In the absence of *Brn3b,* retinal precursors that were originally on an RGC path differentiate into amacrine or horizontal cells and then die prenatally. Additionally, without *Brn3b,* multiple genes were downregulated

and RGC axons elongated towards the wrong intra-ocular and extra-ocular directions. Lastly, when *Brn3b* wasn't expressed, RGC numbers decreased to less than thirty percent of wild type RGC numbers and RGCs expressing *Brn3a* significantly decreased as well (Erkman et al., 1996). On the other hand, in the absence of *Brn3a*, there was a loss of Brn3a-expressing RGCs that would normally stratify in the central boundary between the ON and OFF layers of the IPL. There was also a thirty percent loss in the number of RGCs that were going to express *Brn3a* in addition to a decrease in the number of RGCs expressing *Brn3b*. Overall, the loss of *Brn3a* expression resulted in RGC specification and loss. Also, while the loss of *Brn3a* did not affect central projections, loss of *Brn3b* caused severe defects and a decrease in brain projections (Badea et al., 2009). The loss of *Brn3a* also downregulated the expression of *TrkC*, *Brn3b* and parvalbumin (Huang et al., 2001).

In addition, RGC differentiation and the direction of axonal outgrowth is also regulated by the Sry-related high mobility box (Sox) superfamily of genes. These specifically include the SoxC genes: Sox4, Sox11, and Sox12 (Chang et al., 2017). Also, NEUROG2 is important for early neurogenesis and is expressed prior to the formation of neural lineages. Many studies have shown that NEUROG2 alone could convert iPSCs and embryonic stem cells into neurons (Wang et al., 2017). In chick and mouse models, ATOH7 and NEUROG2 are turned on during early development and work together to differentiate cultured RPE cells into immature RGCs (Hufnagel et al., 2010). Studies have shown that NEUROG2 activates the ATOH7 promoter, but the exact mechanism underlying this is unclear. Studies suggest that via negative feedback, ATOH7 can inhibit NEUROG2 based off NEUROG2's upregulation in ATOH7 mutant retinas (Brodie-Kommit et al., 2021). Following NEUROG2 activation of ATOH7, ATOH7 activates other transcription factors, including ISL1, BRN3B, and BRN3A (to a lesser degree) leading to

RGC fate determination (Wu et al., 2015; Brodie-Kommit et al., 2021; Zhang et al., 2018). ATOH7 binds to sites in the loci of both *Brn3a* and *Isl1*, which suggests the regulation of these two genes by ATOH7 (Brodie-Kommit et al., 2021). The expression of BRN3B and ISL1 can fully compensate for ATOH7 and result in delayed RGC formation; thus, there is a pathway independent of ATOH7 for RGC specification. However, ATOH7 is required for RGC survival as well as axon guidance of RGCs to the optic nerve head. The molecular mechanisms underlying ATOH7's regulation of RGC survival and axon guidance remain unclear. The loss of ATOH7 results in a significant loss of both BRN3A and BRN3B, yet when BAX, a pro-apoptotic protein, is also suppressed, the BRN3A and BRN3B levels are rescued to near-normal levels. While the suppression of both ATOH7 and BAX results in a positive response in the retina to photoreceptor stimulation, significant defects in axon guidance to the optic head ensue (Brodie-Kommit et al., 2021). Additionally, ATOH7 and BRN3B expression together is sufficient reprogram Müller glia to RGCs, a process each transcription factor alone cannot complete (Xiao et al., 2019).

ISL1 plays a role in the specification, differentiation, and maintenance of RGCs, amacrine cells, and horizontal cells in many species (Luo et al., 2019). When ISL1 is inactivated in mouse models, there is a 70% decrease in RGC numbers, and the mice exhibit optic nerve hypoplasia. This loss also results in delayed RGC axon elongation and errors in projection specificity (Xiang et al., 2011). Recent studies have shown that ISL1 and BRN3B form a complex to regulate and co-occupy the promoters of genes necessary for RGC differentiation. The exact mechanism for the ISL1 and BRN3B complex remains unclear (Zhang et al., 2018). BRN3B activates the Shh pathway and represses genes that inhibit RGC development (Xiang et al., 2011).

The SoxC family which includes the Sox4 and Sox11 genes is also important for RGC development. Their loss leads to an absence of RGCs and optic nerve formation (Jiang et al., 2013). The SoxC family also inhibits Hes5, a transcription factor that blocks the differentiation of RGCs, thereby promoting RGC development. Additionally, the SoxC family regulates contralateral (not ipsilateral) RGC differentiation (Chang et al., 2017). Humans contain mostly ipsilateral RGCs, while mice contain mostly contralateral RGCs. **Figure 5** is a diagram that shows the relationship between the transcription factors described above and how their interplay results in RGC differentiation.

Human-induced pluripotent stem cell (hiPSC) technology

Human-induced pluripotent stem cells (hiPSCs) are somatic cells that have been reprogrammed into stem cells that carry properties of self-renewal and pluripotency. Self-renewal means that hiPSCs have replicative immortality through the maintenance of long telomeres; self-renewal allows hiPSCs to be a replenishable and reliable source for research. hiPSC properties of self-renewal also allow the specific targeting and manipulation of the genome through CRISPR engineering tools. Pluripotency means that the hiPSCs have the ability to differentiate into all somatic cell types, except the extraembryonic cells. With a growing knowledge of genes, signal transduction pathways, and epigenetics, novel protocols get established and we have the ability to differentiate hiPSCs into different cell lineages (Singh et al., 2018). Although cells can be grown as a flat monolayer, organoids have also been developed. Since these three-dimensional tissues, or organoids, are similar to tissues and organs *in vivo* in terms of both anatomy and physiology, cell replacement, the field of translational medicine has been revolutionized. hiPSCs can be used for cell replacement, disease modeling, and drug screening, bringing a variety of diseases closer to a cure (Lancaster & Knoblich, 2014).

Clustered regularly interspaced short palindromic repeats (CRISPR) gene editing

Clustered regularly interspaced short palindromic repeats (CRISPR) is a tool for genome editing that consists of a guide RNA (gRNA) and a Cas9 endonuclease (CRISPR Guide). The gRNA has the target sequence necessary to bring Cas9 to a specific region of the genome in addition to the scaffold necessary for Cas9 to bind to the genome. The gRNA is made up of crRNA, an RNA that identifies the genomic target for Cas9, and TracrRNA, an RNA that serves as a scaffold to link the crRNA to the Cas9. The TracrRNA also helps facilitate the processing of pre-crRNA to crRNA. Cas9 (CRISPR Associated Protein 9) binds to the target DNA with the help of the gRNA only when the target sequence is 5' to the PAM (protospacer adjacent motif) sequence. PAM is a short DNA sequence that functions as the binding signal for Cas9. The double-stranded DNA gets cut only when the target site is 5' of the PAM sequence (CRISPR Guide).

A similar enzyme to Cas9 is Cpf1/Cas12a. In a staggered pattern, Cpf1 cleaves DNA and only needs one RNA, which is different than the Cas9 system that requires two. The staggered cleaving pattern is beneficial to genome editing since it allows for directional gene transfer. It is also helpful when targeting non-dividing cells that are challenging to edit through homology-directed repair (HDR). The Cpf1 system also increases the number of CRISPR target sites in the genome that are AT-rich and don't have the PAM sequences utilized by Cas9 (CRISPR Guide).

Endogenous regeneration

Endogenous regeneration is the process by which an organism's cells engage in the repair and regeneration of its own tissue. Endogenous stem cells are adult stem cells that carry properties of tissue specificity, self-renewal and differentiation potential. Most mammals have a very limited innate self-repair potential, which is typically restricted to early development (Xia et

al., 2018). On the other hand, many non-mammalian vertebrates have and maintain this innate self-repair potential throughout their lifetime. The adult zebrafish is experimentally accessible and thus, is one of the major species used to study regeneration. Following injury, adult zebrafish can heal scar-free and regenerate various organs and tissues (Marques et al., 2019). Zebrafish can use their existing Müller glial (MG) cells to regenerate their damaged retina (Xiao et al., 2019). After injury, the MG cells divide and proliferate into a progenitor cell population that can differentiate into many cell types of the retina including rod photoreceptors, cone photoreceptors, retinal ganglion cell precursors, bipolar cells, and amacrine cells (Bernardos et al., 2007; Singhal et al., 2012; Wan et al., 2016; Guimarães et al., 2018; Liu et al., 2019). In addition to the retina, zebrafish can also regenerate their fins, heart, spinal cord and kidney (Beffagna et al., 2019). Studies have also shown that RPE cells in the xenopus can transdifferentiate into different retinal cell types after retinal injury to regenerate the retina (Vergara et al., 2009). Scientists hope to recapitulate the regenerative potential seen in non-mammalian vertebrates by using endogenous stem cells. In order to do so, we need to understand which genes are upregulated and downregulated in the regeneration of specific cell types. We also need to understand the interactions between such genes and how they are regulated.

Signaling pathways in endogenous regeneration

While the underlying mechanisms are unclear, many proneural transcription factors are upregulated following injury during endogenous regeneration. One of these transcription factors is the achaete-schute homolog 1a gene, ASCL1, which activates LIN-28, an mRNA binding protein that promotes pluripotency by suppressing *let-7* miRNA expression (Ramachandran et al., 2010; Madelaine et al., 2017). *Let-7* inhibits the expression of a variety of genes associated with regeneration such as *lin-28*, *c-myc*, *ascl1a*, *pax6b*, *hspd1*, and *oct4* (Ramachandran et al.,

2010); thus, by inhibiting *let-7*, ASCL1 indirectly activates the expression of regeneration-associated genes. ASCL1 helps convert MG cells into cells with stem cell-like characteristics. Also, following injury in their retina, zebrafish overexpress sex-determining region Y-box 2 (SOX2) and ATOH7, both of which are transcription factors and usually expressed in neural progenitors and retinas during early development. The signaling pathway involves SOX2 activating ASCL1 and ATOH7 expression. These two transcription factors (ASCL1 and ATOH7) then induce the expression of LIN-28 (Madelaine et al., 2017).

Initially discovered in drosophila regulating organ size, the Hippo signaling pathway is also conserved in mammals and involved in endogenous regeneration by inhibiting molecules (YAP/TAZ) that lead to this process. Thus, the inhibition of the Hippo pathway causes injured cells to become progenitor-like (Rueda et al., 2019). In the Hippo pathway, the mammalian STE20-like protein kinase ½ (MST1/2) and mitogen-activated protein kinase kinase kinase kinase (MAP4K) phosphorylate yes associated protein (YAP) and transcriptional co-activator PDZ-binding motif (TAZ). YAP and TAZ become inactivated because this phosphorylation prevents YAP and TAZ from translocating into the nucleus. As a result of the inhibition of the Hippo pathway, unphosphorylated YAP/TAZ translocates into the nucleus and binds to the four TEA domain transcription factors (TEAD 1-4) to start transcription. While embryonic stem cells express YAP, differentiated cells do not. During early stages of embryonic development, YAP is highly expressed, yet this halts shortly after birth. However, when tissues are injured, YAP/TAZ expression resumes and rises, leading to dedifferentiation and progenitor cell proliferation (Wang et al., 2017). **Figure 6** illustrates the Hippo signaling pathway. As one can clearly see, the Hippo pathway inactivates YAP/TAZ and thus, inhibits cell reprogramming and regeneration. When

YAP stops responding to Hippo signaling, injured cells become progenitor-like (Rueda et al., 2019).

In addition to the Hippo pathway, fibroblast growth factors (FGFs) play a role in regeneration. FGFs are master regulators of both organogenesis and tissue homeostasis, and are instrumental in the migration, proliferation, differentiation and survival of various cell types (El Agha et al., 2016; Maddaluno et al., 2017). FGFs bind to FGFR1-4, four tyrosine kinase receptors on the membrane, which then results in the activation of various signaling pathways. FGFs are also involved in the development of organs including the brain, muscle, kidney, hair, heart and lung (Kurosu et al., 2007). In mammalian species such as rats, rabbits, dogs and mice, FGF extracts can stimulate wound healing in cornea, cartilage, peritoneum, peripheral nerve, eardrum, striated muscle, duodenal ulcers, salivary glands, tibia, and sternum (El Agha et al., 2016). FGFs play a key role in limb regeneration of axolotls, fin regeneration of zebrafish, lens regeneration of newts and *Xenopus laevis* larvae, neural tissue regeneration in planarians, and retinal regeneration in chick embryos as well as adult zebrafish. FGFs also coordinate with other signaling pathways involved in regeneration, in particular the Wnt pathway, in order to increase the regenerative potential of cells (Maddaluno et al., 2017).

Along with FGFs, the Bone Morphogenic Protein (BMP) signaling pathway is involved in embryogenesis and regeneration. BMPs are within the transforming growth factor β (TGF- β) family with both canonical and the non-canonical mechanisms. The canonical pathway starts with BMP binding to cell-surface receptors to form type I and type II dimers. These dimers are serine/threonine kinase receptors. When BMP binds, these heterotetrametric complexes phosphorylate downstream receptor-regulated Smads (R-Smads), including Smad1, Smad5, and Smad8. These phosphorylated R-Smads combine with Smad4, the co-mediator protein, and

together they translocate into the nucleus to function as transcription factors. BMP also leads to reprogramming in cells that leads to regeneration (Yu et al., 2010). In addition, BMP antagonists, including noggin and chordin, also inhibit BMP (Wang et al., 2014). Studies have shown that the inhibition of BMP results in a decrease in regeneration. For instance, noggin treatment in the muscle tissue of neonatal mice resulted in a lower level of regeneration potential (Costamagna et al., 2016).

Another important pathway in mammalian regeneration is the Wnt signaling pathway. Of the Wnt signaling pathways, there is a canonical Wnt signaling pathway (β-catenin dependent) and a non-canonical pathway that further divides into the Wnt/Ca2+ pathway and Planar Cell Polarity pathway (Komiya et al., 2008). The canonical Wnt signaling pathway (β-catenin dependent) is the one that is most involved in regeneration. It results in the build-up of β-catenin, which translocates to the nucleus and assists in transcription. Without Wnt, β-catenin is degraded in the cytoplasm by the β-catenin destruction complex, which consists of Axin, protein phosphatase 2A (PP2A), adenomatosis polyposis coli (APC), casein kinase 1α, (CK1α), and glycogen synthase kinase 3 (GSK3). When Wnt is present, it attaches to a seven-transmembrane receptor complex that consists of the frizzled receptor (FZD) and low-density lipoprotein receptor-related protein 5/6 (LRP5/6). This causes axin to bind to LRP5/6, which then inhibits the formation of the β-catenin destruction complex and thus, the degradation of β-catenin. A positive feedback loop ensues, and β-catenin accumulates in the cytoplasm. Also, axin binding to LRP5/6 activates the phosphoprotein dishevelled (Dsh), which casein kinase 1α activates. Dsh inhibits GSK3, another factor within the β-catenin destruction complex, so this again leads to a build-up of β-catenin. When β-catenin is accumulated in the cytoplasm, it can translocate into the nucleus with the help of other factors such as Axin. In the nucleus, β-catenin acts as a

transcriptional co-activator by making a complex with T-cell factor/lymphoid enhancer factor (TCF/LEF) and helping in the process of transcription (Clevers, 2006). The canonical Wnt signaling pathway described above is outlined in **Figure 7**. The role of the non-canonical pathway remains unclear despite its involvement in some inflammatory diseases. This pathway is independent of β-catenin and transcription. It regulates polarized organization and directs migration of actin cytoskeleton (Komiya et al., 2008). Also, Wnt signaling is involved in not only species with robust regenerative potential like zebrafish and salamanders but also mammals with limited regenerative potential. The decrease in Wnt signaling leads to the decrease in regenerative potential of the animal as well as a decrease in the recruitment of stem and progenitor cells to the area of injury. For example, when Wnt signaling is halted in zebrafish, an injured fin does not get regenerated as it would in a normal zebrafish (Whyte et al., 2012).

Lastly, the Hedgehog signaling pathway is involved in development and cell differentiation. The Sonic hedgehog (Shh) is the most well-known hedgehog homolog. In studies on axolotls, Shh signaling regulated dorsoventral patterning and was necessary for the regeneration of the tail. As a result of Shh signaling restriction, the axolotl tail was unable to get regenerated following injury (Schnapp et al., 2005). In **Figure 8**, the canonical Shh signaling pathway is outlined. In the canonical Shh signaling pathway, Shh binds to and inactivates Patched (Ptch1), a 12-transmembrane protein that typically works to repress smoothened (Smo) activity. When Shh binds to Ptch1, the resulting inactivation of Ptch1 increases Smo activity. Smo activates many signaling cascades that lead up to the increased activation of glioma-associated oncogene homolog (Gli) proteins Gli1, Gli2, and Gli3 (Carballo et al., 2018). Gli1 is a transcriptional activator, while Gli2 and Gl3 are both transcriptional activators and repressors. Gli2 and Gli3 under normal conditions are truncated on the C terminus and repress Shh target

genes. Gli2 and Gli3 activation by Smo causes them to undergo posttranslational modifications and translocate into the nucleus, where they function as transcriptional co-activators and assist the transcription of Shh target genes, which consist of *Gli1* and *Ptch1*. Gli1 under normal coniditons is not expressed and is produced by the activation of the Shh pathway through Gli2 and Gli3. When activated, Gli1 helps in the process of transcription (Niewiadomski et al., 2019). In addition to transcription, Gli also affects the Wnt pathway by inhibiting β-catenin. The Wnt pathway also affects the Shh pathway, as TCF/LEF upregulate Gli (Carballo et al., 2018).

Cell-based models to explore retinal biology

The retina is a complex, multilayered neural tissue, and thus, there are no practical ways to explore retinal biology in humans. Challenges also consist of the generation of enough specific cell types, the functional integration of transplanted cells, and the delivery of such cells with the absence of an immune response. Cell based approaches might offer a solution. hiPSC technology allows for the formation of organoids, which are three-dimensional tissues that can recapitulate the anatomical structure and physiology of human tissues (Singh et al., 2018).

New innovations in stem cell research offer new models to test RGC protective strategies as well as to study the basic biology of RGC outgrowth and targeting. Studying 3D tissue organoids not only broadens our knowledge of human development but also allows for drug screening and new methods of human disease modeling and repair. The generation of human embryonic and induced pluripotent stem cells can allow for the massive expansion of donor cells that have the potential to differentiate into any type of cell in the body. These pluripotent stem cells can be used for the production of 3D tissue organoids, allowing for the generation of a specific cell-type in both high precision and high amounts. For ophthalmology research, organoid technology has opened up new avenues of studying retinogenesis *in vitro*, including

developmental studies and disease modeling (Wahlin et al., 2017, Llonch et al., 2018). With organoids, we can study early human retinal cell fate decisions, as well as the role of transcription factors during retinal development. We can also use the organoids as a tool to study the progression of retinal disease *in vitro*. Furthermore, the 3D organoids can be used for transplantation and high-throughput screening approaches due to their ability to proliferate and generate highly numbered retinal cell populations (Llonch et al., 2018). With the potential to mimic the structure, function, and organization of the retina, the 3D organoids are useful tools for understanding the molecular mechanisms underlying retinal diseases (Mazerik et al., 2018).

Many optic neuropathies are associated with incorrect synapse formation, inadequate number of RGC axons, and misguided RGC axonal growth from the retina to the brain (Mesentier-Louro & Liao, 2019). Due to a disconnect between the retina and the brain, visual information is not properly transmitted to the brain. With retinal organoids, we may be able to further our understanding of the axonal growth cues and enrich our knowledge on how to steer them in the proper direction. New cell-based models, such as those afforded by organoids, could enable new approaches for sending RGC axons to the brain. The most promising method would be a therapeutic that contains the exact concentrations of attractants and repellents to guide the RGC axons to the brain. With the right amount of guidance cues, the RGC axons would be correctly navigated to the brain and the restoration of sight would occur. This would be a discovery that would one day be able to cure the optic neuropathies that break the connection between the retina and the brain (Amin et al., 2018). In addition, connecting the retina to the brain might increase survival in normal retinal organoids and may allow one to study the role of sensory input to the brain.

Mouse PSC (mPSC)-derived retinal organoid differentiation

The generation of PSC derived retinal cells was a breakthrough initiated by Eiraku and Sasai (Eiraku & Sasai, 2011). His pioneering approach allowed for the modelling of retinal development *in vitro* with mouse embryonic stem cells (mESCs) (Eiraku & Sasai, 2011). In Eiraku's protocol, the retinal organoid formation begins with a reaggregation of a specific number of dissociated mESCs in 96 well plates, which causes embryoid aggregates to form (Eiraku & Sasai, 2011). The addition of Matrigel, which consists of extracellular matrix (ECM) components creates optic vesicle-like structures that express transcription factors like Rx and Pax6 within a week. After 3 days of differentiation, more than half of the structures undergo invagination and form optic cup-like structures, which are separated from the aggregates. These structures consist of an outer nuclear layer with photoreceptors, an inner nuclear layer with horizontal, bipolar, amacrine and Müller glia cells, and a ganglion cell layer (Llonch et al., 2018). Gonzales-Cordero was then able to advance this approach by lengthening the time of the organoids in the extracellular matrix and not performing the dissection of parts of the organoid (Gonzalez-Cordero et al., 2013). In addition to this, parallel studies by Lakowski and Santos-Ferreira added cell surface markers for the separation of rod photoreceptors from retinal organoids (Lakowski et al., 2015, Santos-Ferreira et al., 2016). The advantages to this approach are that now scientists can understand how complex their retinal organoids are and can work towards replicating the anatomical and physiological processes of the retina *in vivo*.

hPSC-derived retinal organoid differentiation

Pluripotent stem cell derived retinal organoids have also been used to study human retinogenesis in ways not previously possible. Although animal models provide us with a greater understanding on RGC growth mechanisms, the way human RGCs respond to molecular cues to

grow towards the brain can be even further studied using human PSC-derived retinal organoids, a reliable model of RGCs development. Many different labs with varying organoids all start off with stem cells and transition into neural progenitors in a self-organizing fashion, progressing to eye-field properties.

Based on their aggregation approach with mouse ESCs, Nakano's group formed a protocol in 2012 that results in the formation of retinal organoids from human ESCs (Nakano et al., 2012). With quickly aggregated hESCs (9000 cells/well) and Matrigel, which consists of ECM parts, optic cups were formed by adding 10% FBS along with Hedgehog agonist, smoothened agonist and a Wnt agonist. These optic cups contained neuroretina and retinal pigment epithelium (RPE) (Nakano et al., 2012). Wnt inhibition is necessary to regulate RPE genes (Llonch et al., 2018).

Other protocols use this aggregate approach as well. In Fligor et al (2018), the hPSCs are lifted from Matrigel-coated wells using dispase and suspended as embryoid bodies (Fligor et al., 2018). These are then moved to a neural induction medium of DMEM, F12 (1:1), N2 supplement, MEM non-essential amino acids, heparin and PSA. Following seven days, the embryoid bodies get plated with 10% FBS in NIM, and after twenty-four hours, the FB gets removed. Following sixteen days of differentiation and cell maintenance, the cell aggregates were lifted and kept in Retinal Differentiation Medium (RDM), a medium that contained DMEM/F12 (3:1), B27 supplement, MEM non-essential amino acids, and PSA (Fligor et al., 2018).

As demonstrated by Wahlin and colleagues, this stem cell forced aggregate approach cause the spontaneous formation of optic vesicles (Wahlin et al., 2017). PSCs maintained in mTsSR1 were used to initiate serum-free embryoid body forced aggregates for optic vesicle

induction. Stem cells were passaged with a longer Accutase incubation for twelve minutes and one thousand cells in fifty microliters of mTeSR and blebbostatin were seeded per well into polystyrene 96-well U-bottom plates. Aggregates were transitioned to BE6.2 medium by adding 50µl+2% MG on day 1 and 1% MG each day thereafter. On days 4 to 8, a 50% medium exchange (100 µl) was performed daily and every other day thereafter. This medium contained 1% MG and 3µM of IWR-1e. At day 10, vesicles were transferred to 15 mL conical tubes, rinsed 3 times in HBSS, and resuspended in BE6.2 + 300 nM Smoothened agonist from days 10 to 12 to improve retinal induction. From days 12 to 18, the medium contained LTR+SAG. From days 10 to 12, sharped tungsten needles were used to excise optic vesicles to prevent overgrowth and necrosis. After day 20, 500nM all-trans retinoic acid was added to the LTR medium to enhance the survival and differentiation of the retinal organoids. By optimizing the growth medium composition, oxygen concentration, and aggregate size, they were able to enhance the generation of optic vesicles. One change was the doubling of the E6 concentration, which improved vesicle morphology. B27 further enhanced the 3D neural vesicle formation. Additionally, aggregates under hypoxic conditions had increased viability due to its effect on improving the pluripotency and proliferation of hPSCs. An important part of this work was that hypoxia increased survival and improved vesicle formation in developing organoids. Blebbistatin, a selective cell-permeable inhibitor of non-muscle myosin ATPase activity, also increased cell survival when passaged to single cell levels (Chen et al., 2010; Walker et al., 2010; Xu et al., 2010). In addition, blebbistatin increased cloning efficiency following dissociation to single cells. Following the continuous removal of non-retinal cup (RC) like structures and the trimming of overgrown vesicles, the 3D RCs became reasonably homogenous after a span of a month. These isolated optic vesicles then transformed into laminated 3D retina cups. Early-stage optic vesicle

formation occurred in twelve days while specific retinal cells were born over a three-month span. This method led to the formation of all retinal types, including photoreceptors, retinal interneurons, ganglion cells and RPE tissues and could be maintained over 300 days.

The other approach, introduced by the Gamm lab, is based on a hybrid 2D-3D system. Briefly, stem cells are mechanically scrapped and embryoid bodies form in suspension in N2 containing neural induction medium. They are then attached to a Matrigel based basement mebrane and grown in 2D until columnar neuroepithelial cells form (Meyer et al., 2009). After six days on this substrate, several eye field markers (e.g., RX, SIX3, SIX6, LHX2, OTX2 and PAX6) were detected by PCR. After ten days, the vast majority of cells tested double positive for Pax6/Rx. The eye-field structures were mechanically detached and stimulated by B27 supplementation that promotes further retinal differentiation. By Days 20 to 25, a couple populations of free-floating neurospheres were shown (Meyer et al., 2011). The retinal neurosphere were then manually separated after day 26 to prevent the instability of the retinal morphology.

As shown by Zhong et al., the aggregate approach was used with major modifications (Zhong et al., 2014). On Day 0, the hPSC were detached using dispase and cultured in suspension with mTeSR1 medium and 10 µM Blebbistatin to cause aggregate formation. The aggregates were then moved into a NIM by replacing the medium on Day 1 with a 3:1 ratio of mTeSR1/NIM, 1:1 on Day 2, and 100% NIM on Day 3. The aggregates were then seeded onto wells coated with Matrigel and containing NIM on Day 7. On Day 16, the NIM was removed and switched to DMEM/F12 (3:1), adding 2% B27, 1x NEAA, and 1% antibiotic-antimycotic (Zhong et al., 2014). On week 4 of differentiation, the neural retina domains were manually separated and cultured in suspension, forming 3D retinal cups. Retinoic acid was added to

promote photoreceptor maturation (Zhong et al., 2014). This new protocol incorporated the attachment of cysts to Matrigel-coated plates and the supplementation of fetal bovine serum (FBS), RA and taurine to promote photoreceptor development and maturation, resulting in rho^{+}, S-opsin^{+} and L/M-opsin^{+} photoreceptor generation (Zhong et al., 2014). Using this protocol, retinogenesis spanned across weeks five to twenty-two (Zhong et al., 2014). Overall, this 3D organoid technology greatly improved the availability of human retinal tissue and human photoreceptors.

Advances and limitations of organoid technology

Some advances of the organoid technology include our ability to study gastrulation, morphogenesis, and organogenesis in the human eye. Organoid technology allows us to study human biology, which is typically difficult since humans are not experimental models. Organoids have been used as not only drug screeners, but also a tool to understand human development and disease (Holloway et al., 2019). For example, patient-derived 3D liver cancer organoids have been used as a drug screening platform to test their responses to 129 cancer drugs (Li et al., 2019). While there has been remarkable progress in organoid technology, organoids are still primitive and lack many essential features found in the native tissue. They are also heterogeneous, which makes them similar but different from native tissue found in the human body (Holloway et al., 2019). Unguided organoids, which are organoids that spontaneously undergo morphogenesis and differentiate, have been shown to generate high variability (Qian et al., 2019). Guided organoid methodologies address these concerns and use growth factors to differentiate organoids towards desired lineages, thereby increasing complexity. These methodologies include the addition of small molecules and growth factors to the organoids to facilitate the differentiation process (Qian et al., 2019).

Bioreactors have also been used to increase nutrient and oxygen diffusion and maintain 3D suspension culture (Clevers et al., 2017). However, bioreactors are bulky and consume much culture medium, which decreases the efficiency of the organoid system. Neurons generated in organoids parallel the development and maturation of neurons as they develop in the embryonic stages *in vivo.* Organoids can also showcase cell-type diversity by producing a variety of different cell-types (Qian et al., 2019). However, because they are made *in vitro*, they do not contain all the cell types of the actual organ (Clevers et al., 2017). For example, while the retinal organoids have photoreceptors, bipolar cells, retinal ganglion cells, horizontal cells and amacrine cells, they do not contain the RPE needed for PR function along with blood vessels. A way to avoid such a challenge is by artificially combining separately cultured cell types. Co-culture systems have been implemented to further improve upon the complexity of organoids and mimic the organogenesis that occurs. Additionally, organoids have been able to produce similar levels of gene expression as that of human fetal tissues. Nevertheless, we must be cautious when directly extrapolating gene expression analysis to function (Qian et al., 2019).

There have been many breakthroughs in organoid technology, including the successful treatment of certain diseases with cultured organoids. Organoids are tools that have allowed for the integration of various technologies including gene editing, imaging, NextGen sequencing, artificial intelligence, bioengineering and more (Clevers et al., 2017). This integration of various technologies is what makes organoids unique. Its disease modeling applications have also been very successful, demonstrating that organoids can model various disorders. The structural sophistication of organoids is one of the main advantages of organoids, as it allows us to study their progression through multiple lineages in a process that mimics the development of the native tissue (Clevers et al., 2017). As mentioned previously, organoids bring up a challenge of

variability. In order to reduce this variability, defined progenitors should be used instead of pluripotent stem cell aggregates. Also, the culture medium and matrix should be fully defined. High resolution non-invasive sensing technology with monitoring parameters like temperature, pH, proteins, oxygen and morphology, alongside a machine learning process can optimize the cell culture and minimize variability as well (Clevers et al., 2017). Partial automation and the improvement of delivery logistics in terms of preservation and transport of organoids should also be put into effect in order to optimize the target tissue isolation. Similar to native organs, organoids are able to get constructed with minimal exogenous interference and can reform many complex interactions within the organ they are modeling. Because of their plasticity, they are reliable tools for drug screening. Due to the complexity of their development, organoids experience much heterogeneity, which could pose as a problem. Guidance cues and growth factors can be used to facilitate the growth of the organoids and reduce this randomness that may arise (Clevers et al., 2017).

In 2011, the first stratified cell-specific layered organization from mESCs was formed. Optic-cup vesicles were generated as a result of evagination and invagination steps, and later underwent morphogenesis similar to *in vivo* retinogenesis (Nakano et al., 2012). Later, as a result of the addition of extrinsic factors such as Wnt antagonists, Shh, and FGF, retinal organoids showed a more stratified neural morphology and formed chemical and electrical retinal synapses (Nakano et al., 2012; Eguizabal et al., 2011). Trisectioning of organoids also resulted in an increase in the overall quantity of retinal organoids as well as the number of photoreceptors (Völkner et al., 2016). In 2014, outer segments which include the light-sensitive photoreceptors were found in 3D retinal organoids, from which functional light responses were recorded.

Markers for the phototransduction protein (recoverin) as well as the synaptic vesicle protein seen in rods (Zhong et al., 2014).

In order to increase survival rates of these organoids, culture conditions were improved upon using a bioreactor. The retinal laminar stratification also improved and high numbers of photoreceptors with cilia were produced (DiStefano et al., 2018). New approaches to combat the absence of a vascular system within organoids include the use of hydrogels and addition of insulin growth factor 1 (IGF1) to the media which accelerated maturation of photoreceptors with RGCs. Hydrogels enhance the RPE pigmented phenotype, function as scaffolds and can deliver cells into the retina, driving neural and retinal differentiation under 3D conditions. Because these approaches improved the vascular system of these organoids, the photoreceptors morphologically exhibited maturation and co-cultured RPE interactions showed enhancements. Evenly distributed photoreceptors were found in the outer retina at days 120-160, a time frame that correlates to *in vivo* human retinogenesis (Hunt et al., 2016).

Current limitations of retinal organoid models

Although retinal organoids are highly promising, this technology is faced with some limitations. Although a major symptom of retinal disease is the loss of visual function, retinal organoids tend to show only weak responses to light (Zhong et al., 2014). This may be due to the limited development of the outer segment discs (visual pigments and phototransduction proteins) and thus, lack of interaction with the RPE. Also, there is retinal ganglion cell death in retinal organoids as a result of the absence of connections to the brain. Thus, functional retinal circuits do not form (Kaya et al., 2019).

In addition, current retina organoids are not as complex and fully mature as their counterpart (Capowski et al., 2019). Current retinal organoids do not possess cell type diversity,

are variable in their development, carry hiPSCs line-to-line variability, and are not consistent in lamination patterns (Kaya et al., 2019; Kim et al., 2019; Capowski et al., 2019). Also, in order to form vascularized tissue seen in retinal tissue *in vivo*, 3D retinal organoids must contain endothelial cells. The immune system is also a factor in retinal degeneration, specifically the inflammatory aspects, and so the 3D retinal organoids must be co-cultured with patient-derived microglial cells to understand this interaction. A functional layer of RPE is also crucial for 3D retinal organoids as that would make the organoid more physiologically similar to retinas *in vivo*; the RPE is required for maintaining the visual cycle due to its role in retinoid recycling (Capowski et al., 2019).

Other challenges include shortening the time it takes to generate 3D retinal organoids that contain photoreceptors (Capowski et al., 2019). Additionally, reproducing aging effects in 3D retinal organoids for the disease modeling of late-onset retinal diseases poses a challenge. The morphology of the photoreceptor outer segments in retinal organoids is immature and while similar to those in fetal development, they are vastly different than those in the mammalian adult retina, which are more complex in their morphology, stratification and function (Masland et al., 2012). Similar developmental timing in retinal organoids as *in vivo* is crucial for the study of late-stage processes like late-onset retinitis pigmentosa (RP). RP occurs mainly in the elderly and so having a model that can mimic such developmental processes is necessary for its study. Strategies to mimic neurodegenerative late-onset diseases such as the addition of stressors in culture medium, Progerin overexpression, and telomere shortening have been used in Parkinson disease cellular models, but these approaches have not yet been used in 3D retinal organoids (Castro et al., 2019). These limitations are obstacles to studying therapeutic strategies for retinal diseases that warrants further research effort.

Transdifferentiation of neuronal cells from human pluripotent stem cells

The study of optic neuropathies can be substantiated using retinal organoids that can mimic the development and degeneration of the retina. This project provides a novel therapeutic strategy for optic neuropathies such as glaucoma by using endogenous regeneration to regenerate RGCs that were formerly assumed irreversibly lost. My hypothesis was that the endogenous regeneration seen in the zebrafish can be recreated in the human eye to form new RGCs by ectopically overexpressing specific transcription factors involved in RGC specification and differentiation. Our results suggest that the overexpression of four specific transcription factors, NEUROG2, ATOH7, ISL1, and BRN3B, converted undifferentiated human stem cells into retinal ganglion cells with long branched neurites. Experiments have verified that the differentiated neurons express markers typical of retinal ganglion cells, most notably the POU4F1 (BRN3A). This shows that BRN3A plays a role in human RGC development as well as in the hiPSC-differentiated RGCs.

RESULTS AND DISCUSSION

The overarching goal of this project was to gain a deeper understanding of RGC development, particularly the factors involved and the relationship between them. We hope that by understanding the basic science behind RGC development using CRISPR gene editing tools and the process of endogenous regeneration, we will be one step closer to developing novel therapies that will prevent, minimize, or even restore vision loss due to RGC degradation. The focus of my thesis was to understand the involvement of BRN3A in RGC development as well as its role in the NEUROG2, ATOH7, ISL1, and BRN3B pathway.

Design of transgene constructs for fluorescence markers

An aim of my project was to utilize a tool that would cause stem cells to differentiate into RGCs which could be used as a proof-of-concept for minimal transcription factor cassette capable of eventually transdifferentiating into RGCs. To verify the formation of RGCs and analyze their complexity, we first generated cell based RGC reporters, which gave a dynamic live cell readout. These reporters were created by coupling fluorescent protein expression to endogenous retinal genes. To accomplish this, we used CRISPR targeting tools that carry the RGC markers POU4F1 (BRN3A) and POU4F2 (BRN3B). Synaptic protein reporter tools (e.g., DLG4 and CtBP2) were also made to highlight functional connections between retinal cells.

The plasmid construct used to label RGCs that express BRN3A contained the mNeonGreen fluorescent protein sequence, a myristoylation tag sequence, and a p2A sequence, all three of which surrounded by the homology arms for BRN3A. This plasmid construct is shown in **Figure 9**. The myristoylation tag is a lipid modification that anchors the mNeonGreen fluorescent protein to the membrane of the cell (Maurer-Stroh et al., 2002). A porcine 2A (p2A) sequence consists of a twenty-two amino acid polypeptide that causes ribosomal skipping during

protein translation. This allows a single mRNA transcript containing BRN3A and mNeonGreen to create separate functional proteins (Daniels et al., 2004).

The plasmid construct used to label RGCs that express BRN3B contained the tdTomato fluorescent protein sequence, two p2A sequences and one Thy1.2 sequence. The P2A sequences that induce ribosomal skipping result in the formation of separate and functional BRN3B, tdTomato, and Thy1.2 proteins. The Thy1.2 sequence codes for the glycosylphosphatidylinositol (GPI)-anchored protein, allowing for the localization of the tdTomato fluorescent protein into the outer leaflet of lipid rafts in the cell membrane (Haeryfar & Hoskin, 2004). This feature allows us to selectively isolate the cells via immunostaining. This plasmid construct is also shown in **Figure 9**.

Furthermore, plasmid constructs used to label synaptic proteins, C-terminal binding protein (CtBP2) and Discs Large 4 (DLG4)/post-synaptic density-95 (PSD-95), were made. CtBP2 codes for a synaptic ribbon at presynaptic active zones of sensory neurons such as retinal photoreceptor cells and bipolar cells (Vaithianathan et al., 2013). DLG4 codes for postsynaptic densities in photoreceptors and bipolar cells (Koulen et al., 1998). One of the plasmid constructs for CtBP2 contained the tdTomato fluorescent protein sequence flanked by the homology arms of CtBP2. The homology arms are included in the plasmid for the purpose of homology directed repair (HDR). After Cas9 makes a cleavage in the target site of the genome, HDR will follow and will use the homology arms of the plasmid to repair the cleavage. Through this repair, the desired sequence containing the fluorescent protein will integrate into the genome. Another plasmid construct for CtBP2 contained the GFP fluorescent protein flanked by the homology arms of CtBP2. Furthermore, one of the plasmid constructs for DLG4 contained the tdTomato fluorescent protein flanked by the DLG4 homology arms. Another plasmid construct for DLG4

contained the GFP fluorescent protein flanked by DLG4 homology arms. The plasmid maps for DLG4-tdTomato, DLG4-GFP, CtBP2-tdTomato, and CtBP2-GFP are also shown in **Figure 9**.

Some modifications that have been done over the past year on these CtBP2 and DLG4 plasmids were the replacement of the gRNA scaffold V1 with gRNA scaffold V3. gRNA is composed of the gRNA scaffold, a sequence necessary for Cas9 binding, and approximately twenty nucleotides that define the target sequence of the genome. This new scaffold was more robust and increases transfection efficiency. Another modification was the replacement of SV40 with eHRE. SV40 allows for the nuclear import of a plasmid carrying sequences of interest (Prasad & Rao, 2005). HRE is a hypoxia response element that increases expression of a gene in respond to hypoxia. Both SV40 and HRE are DNA tagging sequences. I switched the SV40 with HRE to transcription efficiency (Tang et al., 2002). This was something we wanted to explore as we were not certain if the switch would improve the transfection.

After assembling and Sangar sequencing the final product of the CtBP2-GFP plasmid, I discovered a frameshift mutation that resulted in a premature stop codon in the GFP transcript. To correct this mutation, we carried out site directed mutagenesis. Using oligonucleotide primers that contained the corrected sequence, I PCR amplified entire plasmid and re-circularized the plasmid using Gibson assembly. Once PCR amplified, the plasmid was switched back together by Gibson assembly. Gibson assembly is an isothermal reaction that uses 5’ exonuclease, DNA polymerase, and DNA ligase enzymes to chew back overlapping ends, fill in gaps and ligate DNA fragments respectively. Following the completion of the Gibson assembly, the reaction product was restriction enzyme digested with a methylation specific DPN1 enzyme. This enzyme functions to degrade the original, unmodified plasmid template and thus, make sure that all that the final product is the desired, modified plasmid. It does so by cutting up the plasmid that

contains methylation. The original plasmid is coated in methyl groups because methylation gets added in bacterial replication, and so the DPN1 enzyme degrades this plasmid. The final, modified plasmid is methyl free because there are no methyltransferases in replication done in PCR. Sequence verification of the DLG4-p2A-GFP, and DLG4-p2A-tdTomato are shown in **Figure 10**, while that of CtBP2-p2A-eGFP, CtBP2-p2A-tdTomato plasmids are shown in **Figure 11.**

Transgene construct transfection and generation of reporter cells (BRN3A-Neon, BRN3A-Neon & BRN3B-tdTomato, and CtBP2-tdTomato)

Once we had successfully constructed and sequence verified CRISPR Donor vectors for gene verification, we then sought to integrate these cassettes into human pluripotent stem cells. This was accomplished by transfecting the plasmids into a human induced pluripotent stem cell line (IMR90.4) to generate reporter cells. The Brn3a-Neon and CtBP2-tdTomato plasmids were first transfected into individual cell lines. Once the Brn3a-Neon cell line was verified, BRN3B-tdTomato was transfected into the Brn3a-Neon cell line to generate a dual RGC reporter. The day before the transfection, the cells were doxy-treated to turn on Cas9 and thus allow for the CRISPR/Cas9 gene editing. To briefly discuss the process of transfection, cells were single cell passaged with Accutase when the stem cell colonies were at high density (around 100,000 to 200,000 cells). The cells were then resuspended in hypoosmolar electrolytic solution and plasmid in various concentrations. They were then electroporated with one pulse at 1300 V for 20 ms and immediately and very gently transferred to the surface of a single well in a Matrigel coated 12-well plate. Transfection of plasmid DNA leads to a heterogeneous mixture of unmodified cells and modified gene edited cells. To identify modified colonies, genotyping was carried out for most of the cell lines, except CtBP2-tdTomato. The CtBP2-tdTomato cell line did not require

genotyping since the CtBP2 gene is expressed in stem cells. Thus, using fluorescent microscopy, the tdTomato signal was visualized in some of the colonies. A figure that illustrates the fluorescence of the CtBP2-tdTomato colony is shown in **Figure 12**.

The BRN3A-Neon and BRN3B-tdTomato cell lines required genotyping. To briefly describe the process of genotyping, following transfection, cells were colony picked onto a 48-well plate and then expanded via non-enzymatic cell dissociation buffer (CDB) passaging. They were spun down in a 96 well plate and lysed to extract their DNA with Quick Extract (QE) buffer. After an hour of incubation, the DNA was diluted in Tris-low EDTA (pH 8.0) diluted 1:1 in nuclease free water. The DNA was then spun down and transferred into a new 96 well plate for PCR. This was done to remove the cell debris. Phusion, nuclease free water, and primers were added to each well using conditions that are outlined in the Materials and Methods section. For first pass genotyping to identify the presence of insertion, oligos were used such that one was outside of a homology arm and another within the unique fragment. PCR amplification only occurs if the desired fragment is integrated into the genome. Thus, visualizing the band with the expected size in the gel suggested stable integration of the fluorescent protein into the genome. For second pass genotyping to identify insertions at one or both alleles, the goal was to discriminate between a heterozygous and homozygous insertion of the transfected genes. A heterozygous insertion meant that the transfected gene was only inserted into one of the two chromosomal alleles, while a homozygous insertion meant that the transfected gene was inserted into both alleles. The oligos for second pass genotyping were chosen by having the first be inside the homology arm while the second be outside of the other homology arm. **Figure 14** illustrates how the oligos are chosen for first pass and second pass genotyping. After genotyping the BRN3A-Neon and BRN3B-tdTomato dual reporter cell line, BRN3A-Neon was found to be

homozygous while BRN3B-tdTomato was found to be homozygous. Generating the BRN3B-tdTomato cell line took some additional steps. Originally, we thought that there was a heterozygous insertion of P2A-tdTomato-P2A-Thy1.2 into the BRN3B gene. However, the difference in intensity of the bands in our gel for second pass genotyping suggested that this was a mixed heterogeneous population and so we conducted further colony-picking and genotyping to reselect for a homogeneous population. This process led us to purify the population into a homozygous clone. The genotyping gels for BRN3A-Neon and BRN3B-tdTomato are shown in **Figure 14**.

Following PCR verification of the BRN3A-Neon and BRN3B-tdTomato dual reporter, we further sequence verified each target gene. For both cell lines, the PCR products for second pass genotyping were purified using a Zymo-25 DNA Clean & Concentrate kit and sequence verified. **Figure 15** shows the Sanger sequencing verification of the homozygous insertion of Neon-Myristoylation Tag-P2A into the BRN3A gene. Using the Geneious software package (Biomatters), a contig assembly was generated and aligned sequences were graphically represented to show overlap coverage between the Sanger sequenced files and the expected mNeonGreen-MyrTag-p2A-BRN3A. **Figure 16** illustrates the Sanger sequencing verification of the homozygous insertion of P2A-tdTomato-P2A-Thy1.2 into the BRN3B gene.

NAIB construct transfection and overexpression for RGC generation

To differentiate the BRN3A-Neon and BRN3A-Neon/BRN3B-tdTomato dual reporter cell lines into RGCs, I transfected a NAIB plasmid construct to overexpress transcription factors necessary for RGC development. It contained four RGC promoting genes (NEUROG2, ATOH7, ISL1, and BRN3B), each separated by a p2A sequence enabling polycistronic expression of genes via ribosome skipping. NEUROG2 drives early neural induction, ATOH7 and ISL1 lead to

RGC commitment, and BRN3B causes RGC differentiation (Hufangel et al., 2010; Wu et al., 2015). The NAIB cassette is controlled by a third-generation (3G) tetracycline (TET) activated response element (3G-TRE) and a constitutively expressed reverse tetracycline trans-activating sequence (rtTA). Under a chicken beta-actin hybrid (Cbh) promoter, a constitutively active TagBFP2 sequence is included in the plasmid construct to visualize gene integration. A zeocin selectable marker is present to select against unmodified cells to obtain a pure population of NAIB integrated cells. Along with the NAIB plasmid, the Cpf1 expressing pY026 plasmid was also used. This plasmid co-expresses a Cpf1 enzyme and a CLYBL safe harbor targeting guide sequence. Because the cells already contained a Tet-inducible Cas9 and rtTA, this was necessary as the addition of doxy to induce endogenous Cas9 present in Cas9 engineered cells would inadvertently cause the premature activation of the NAIB cassette. The Cpf1 expressing pY026 plasmid allows us to generate a stable stem cell line. The plasmid maps for both NAIB and the Cpf1 expressing pY026 plasmid are shown in **Figure 17**.

The NAIB and Cpf1 expressing pY026 plasmids were transiently transfected into the BRN3A-Neon hiPSC cell line (IMR90.4) to induce transdifferentiation by BRN3A for live cell imaging of RGCs. The transient transfection resulted in the entry of the NAIB cassette into the cell; however, at this stage, it was not yet stably integrated into the genome. The same transfection process detailed above was carried but with additional zeocin selection for one week, starting with a lower concentration (1:2000) to a higher concentration (1:500). To verify the stable integration, I visualized the constitutively expressed mTagBFP2 signal was visualized by fluorescent microscopy. **Figure 18** shows successful integration of the NAIB cassette into cells.

After the zeocin selection and NAIB integrated enrichment, doxycycline induction was carried out to trigger neuronal and eventually RGC differentiation. After four days of doxycycline treatment (1 µg/ml), cells showed a dramatic shift towards a neuronal morphology compared to controls as shown in **Figure 19**. Four (**Figure 19D**) and five days (**Figure 19E**) of doxycycline treatment (1 µg/ml) showed clear neuronal morphology with phase bright cell bodies (**Figure 19 D-E**, see black arrows) and elongated neurites (**Figure 19 D-E**, see white arrows). In addition to morphological changes, BRN3A-Neon+ cells were observed in the doxycycline treated cells and displayed neuronal morphology with extended neurites (**Figure 20 D-F**, see arrows). The non-doxycycline treated cells did not express BRN3A-Neon (**Figure 20 A-C**). An interesting observation was that some of the neurites expressed BRN3A-Neon while others did not, which suggests the differential expression of BRN3A in different RGC subtypes. Because some of the doxycycline-treated cells expressed BRN3A-Neon, this also suggests that BRN3A plays a role in the relationship between NEUROG2, ATOH7, ISL1, and BRN3B, as their overexpression resulted in the expression of BRN3A.

To further explore the relationship between BRN3B expression and regulation of the endogenous BRN3A gene, we co-transfected the NAIB and Cpf1 expressing pY026 plasmids into the BRN3A-Neon and BRN3B-tdTomato dual reporter hPSC cell lines. The NAIB experiments carried out for the BRN3A-Neon hPSC cell line will be repeated for this dual reporter cell line. By comparing the number of doxycycline cells that express BRN3A-Neon, BRN3B-tdTomato, or both, we will better understand how these two factors, particularly BRN3A, lead to RGC development and how they interact with one another in RGCs. Additionally, I am constructing a plasmid that carries the NAIP1 cassette, overexpressing NEUROG2, ATOH7, ISL1, and BRN3A (POU4F1) in the presence of doxycycline. This

plasmid functions the same as the NAIB plasmid, but instead of a BRN3B (POU4F2) coding sequence, it contains the BRN3A (POU4F1) coding sequence. In the future, we hope to transfect this plasmid into the dual reporter BRN3A-Neon and BRN3B-tdTomato hPSC cell line and conduct the NAIP1 experiments, where we induce the cells into becoming RGCS via doxycycline treatment. By comparing the results of the NAIP1 and NAIB experiments that used the same dual reporter BRN3A-Neon and BRN3B-tdTomato hPSC cell line, we will expand our knowledge on the role of BRN3A in RGC development.

In the future, the overexpression of NEUROG2, ATOH7, ISL1, and BRN3A/BRN3B could become a therapeutic strategy for restoring the RGCs that were previously thought to be irreversibly lost, revolutionizing the field of ophthalmology. We hope that a deeper understanding of RGC development, particularly the transcription factors involved, will help scientists develop novel therapies that will prevent, minimize, or even restore vision loss due to RGC degeneration.

MATERIALS AND METHODS

Cells. IMR90.4 iPSCs (from WiCell) were used for the following study. Cells were routinely tested for mycoplasma by PCR. PSCs were used with approval from the UC San Diego Institutional Review Board.

Cloning. See **Table 1** (Table 1) for a complete list of oligos.

Constructs for generating Tet-inducible HF-iCas9 Cells. The laboratory previously created inducible Cas9 PSCs to facilitate gene-editing. The method is briefly described here. To create HF-ieCas9 cells we targeted the AAVS1 safe harbor site inserting a reverse tetracycline-controlled trans-activator (rtTA) expression cassette at one allele and a 3G-TET regulated eSpCas9 at the other. When bound to doxycycline, constitutively expressed rtTA binds to the Tet operator and ieCas9 expression is induced. The rtTA coding sequence was provided by AAVS1-Neo-M2-rtTA plasmid (Addgene; #60843) whereas the ieSpCas9 coding sequence was amplified from eSpCas9(1.1)(Addgene #71814) (6) and cloned into the AAVS1-puro-Cas9 donor (Addgene #58409) . Briefly, the AAVS1 donor shell was amplified with Phusion Polymerase (#F548L; Invitrogen) using the oligos Cas9backbone_F and Rev and the ieSpCas9 insert was amplified using the oligos Cas9insert_for and Cas9insert_rev. PCR products were cleaned using DNA Clean and Concentrator-5 columns (#D4014; Zymo Research) and donor and insert PCR products were fused together using Gibson assembly reagents (#E2611S; NEB), followed by overnight digestion with Dpn1 enzyme (#R0176L; NEB) to remove parental template DNA. The Gibson product was transformed into chemically competent Stable *E. coli* cells and colonies were miniprepped and verified by Sanger sequencing. For the AAaVS1 targeting, phosphorylated an oligo duplex of the AAVS1_esp_T1 forward and reverse oligos were ligated into BbsI cut pSpCas9(BB)-2A-puro (PX459) V2.0 backbone (Addgene #62988) using Quick

ligase (NEB according to the manufacturer's specifications).

Single-cell passage and maintenance of hiPSCs. Stem cells were maintained antibiotic free on 1% (vol/vol) Matrigel(MG)-GFR™ (#354230; BD Biosciences) extracellular matrix (ECM) coated dishes at 37°C under hypoxic conditions (10% CO_2/5%O_2) in mTeSR1 (Stem Cell Technologies) as previously described (40-43). Cells were passaged every 4-6 days, with Accutase (#A6964; Sigma) for 10-12 minutes, dissociated into single cells, quenched with mTeSR1 plus 5μM blebbistatin (B; #B0560; Sigma), pelleted at 80 x *g* for 5 minutes, resuspended in mTeSR1+B and plated at 2,000 cells per single well of a 12-well plate. After 48 hours, cells were fed with mTeSR alone.

NAIB construct. The NAIB construct was made by a former lab member (Ryan M. Wong) by amplifying four genes (NEUROG2, ATOH7, ISL1 and BRN3B) from cDNAs from day 18 optic vesicles and gDNA. NEUROG2, ISL1, and BRN3B were all amplified from cDNA while ATOH7 was amplified from gDNA. When preparing cDNA, total RNA was extracted from differentiated organoids and reverse transcribed in a 20μl reaction using Superscript IV reverse transcriptase according to manufactures recommendations. Once the cDNA was prepared, it was used as the template for PCR amplification using Phusion Flash High-Fidelity PCR Master Mix (#F548s; Thermo Fisher Scientific). After each gene was amplified, it was run on a 1% agarose gel to confirm that the PCR product was a clean band at the desired size. Once the PCR product was confirmed to be the correct size, the PCR product was purified with the DNA Clean & Concentrator-5 (#D4013; Zymo Research). Following DNA purification, the genes were cloned into a linearized backbone (from above) and Gibson assembled using 20-30 base pair overlap with HiFi DNA Assembly Mastermix (#E2621S; NEB). The plasmid was then digested using Dpn1 enzyme (#R0176L; NEB).

NAIP1 construct. To swap the BRN3B (POU4F2) coding sequence with the BRN3A (POU4F1) coding sequence, the NAIB construct was used as the template for the shell. For the PCR amplification of the shell, two oligos that flanked the BRN3B coding sequence were used. For the PCR amplification of the insert, which would be the BRN3A coding sequence, genomic DNA was used as the template. Phusion Flash High-Fidelity PCR Master Mix (#F548s; Thermo Fisher Scientific) was used for both PCR amplifications. After the shell and insert were both amplified, it was run on a 1% agarose gel to confirm that the PCR product was a clean band at the desired size. Once the PCR product was confirmed to be the correct size, the PCR product was purified with the DNA Clean & Concentrator-5 (#D4013; Zymo Research). Following DNA purification, the genes were cloned into a linearized backbone (from above) and Gibson assembled using 20-30 base pair overlap with HiFi DNA Assembly Mastermix (#E2621S; NEB). The plasmid was then digested using Dpn1 enzyme (#R0176L; NEB).

CtBP2-GFP, CtBP2-tdTomato, DLG4-GFP, and DLG4-tdTomato construct modifications. The CTBP2-GFP, CtBP2-tdTomato, DLG4-GFP, and DLG4-tdTomato constructs (which were made previously in the lab by Anna Ogata) were first modified by swapping the gRNA scaffold V1 with gRNA scaffold V3. Two oligos containing the desired gRNA scaffold V3 sequence and bases complementary to the original gRNA scaffold V1 sequence were used for PCR amplification. The original plasmid was the template. Phusion Flash High-Fidelity PCR Master Mix (#F548s; Thermo Fisher Scientific) was used for PCR. After the PCR product was amplified, it was run on a 1% agarose gel to confirm that the PCR product was a clean band at the desired size. Once the PCR product was confirmed to be the correct size, the PCR product was purified with the DNA Clean & Concentrator-5 (#D4013; Zymo Research). Following DNA purification, the genes were cloned into a linearized backbone (from above) and Gibson assembled using 20-

30 base pair overlap with HiFi DNA Assembly Mastermix (#E2621S; NEB). The plasmid was then digested using Dpn1 enzyme (#R0176L; NEB). After this modification was confirmed, both constructs were modified further by swapping the SV40 with eHRE. The same process described above took place, except the two oligos now contained the desired eHRE sequence and bases complementary to the original SV40 sequence for PCR amplification. Both swaps involved the process of site-directed mutagenesis and generated a more robust plasmid to raise transfection efficiency.

Plasmid preparation for transfection. For routine growth of plasmids, we used chemically competent Stable *E. coli* cells (#C3040I; NEB). DNA for transfection was prepared using the PureLink Fast-Low Endotoxin Midi Plasmid Purification Kit (#210015; Invitrogen) or PureLink HiPure Plasmid Midiprep Kit (#210004; Invitrogen). Plasmids used for quantitative studies of HDR efficiency were never thawed more than 3 times to prevent unwanted degradation of plasmids.

Transfection by electroporation. Cells at approximately 50% confluence were treated overnight with 1μg/ml of doxycycline and passaged with Accutase (#A6964; Sigma) for 12 minutes, dissociated to single cells, quenched with mTeSR1 plus 5μM blebbistatin (B; #B0560; Sigma), pelleted at 80xg for 5 minutes, and resuspended in mTeSR1+B (38). 100,000-200,000 HF-iCas9 iPSCs transferred to a 1.5 ml screw cap tube and spun at 80xg for 5 minutes followed by aspiration to remove all residual liquid and cells chilled on ice for 15 minutes more to improve survival. Cells were quickly resuspended in 10 μl's of R-buffer containing 3μg's of DONOR plasmid and electroporated with a Neon transfection system (#MPK5000; Invitrogen) with the following settings: (1300V, 20ms, 1 pulse). Cells were gently plated into mTeSR1+B+doxy in matrigel coated 12 well plates and grown at 37C under hypoxia. After 48 hours, cells were fed without B.

Genotyping. See **Table 2** (Table 2) for a complete list of oligos. Once cells were transfected into a 12 well plate, the media was aspirated, and cells were treated with mTeSR1+B for 10 minutes. Cells were scraped with a cell scraper and transferred with a P20 pipette tip to a new well in a 48 well plate. Once the colonies were grown to about 50% confluent in 10X magnification field of view, they were expanded by passaging with non-enzymatic cell dissociation buffer (CDB) for seven minutes. The CDB was then removed and replaced with 200 µL of mTeSR1+B. Using the multichannel pipette, the media was blasted into the well up and down two to three times. Half (~100 µL) was transferred to a new well of a 48-well plate for maintenance and half to a semiskirted 96 well PCR plate for first pass genotyping. The 96 well PCR plate was spun down at 13,000 g for 10 minutes and then using the 200 µL Liquidator, 80% of the supernatant was removed. 100 µL of PBS was added to each well, and then the plate was spun down again at 13,000 g for 10 minutes after which 80% of the supernatant was removed again using the liquidator. Next, 20 µL of Quick Extract (QE) buffer was added to each 5 to 10 µL cell remaining solution. The resulting samples were then incubated at 65C for 45 minutes, followed by 98C for 15 minutes. A heating lid was used and periodic vertexing was done on the plate every fifteen minutes during the incubation period. 70 µL of Tris-low EDTA (pH 8.0) diluted 1:1 in nuclease free water was then added to the samples, followed by vertexing the plate for 15-30 seconds to mix it well. The samples were spun down again and then the top half that contained the genomic DNA was transferred to a new 96-well plate. 6 µL of this genomic DNA was used as the template for PCR amplification in which Phusion Flash High-Fidelity PCR Master Mix (#F548s; Thermo Fisher Scientific) was utilized. For first pass genotyping, the oligonucleotides were chosen by having one outside of a homology arm and the other inside of the unique fragment. After the PCR products were amplified, they were run on a 1% agarose gel to determine which wells contained a clean band at the desired

size. To conduct second pass genotyping, the ones that contained the insert in the 48-well plate were single cell passaged using accutase into a 12-well plate. After waiting for the cells in the 12-well plate to grow large enough, they were colony picked into a new 48-well plate. The next steps were identical to what had been done for first pass genotyping. The only difference for second pass genotyping is the choice of oligonucleotides. For second pass genotyping, two oligonucleotides are chosen such that one is outside of a homology arm while the second is inside of the other homology arm. The two oligonucleotides could both be placed within the homology arms to decrease the amplification size and make the PCR easier, but it could lead to false positives if used too early in the colony screening process when the plasmid is still present. In the gel, there are three possible results that can be seen: a band for the insert, a band for no insert, and two bands for both insert and no insert. If only a band for the insert is seen, then the cell line is homozygous for that insertion. If only a band for no insert is seen, then that cell line is unmodified and does not contain the insertion. If both a band for the insert and a band for no insert is seen, then that cell line is heterozygous for that insertion, as one chromosome as the insert and the other does not.

Generation of BRN3A-Neon integrated pluripotent stem cells. The BRN3A-Neon construct was transfected into stem cells. Cells were electroporated at 1,300V for 20 ms. After transfection, genotyping and sequence verification followed to select for the cells that had stably integrated the genetic cargo.

Generation of dual reporter BRN3A-Neon and BRN3B-tdTomato integrated pluripotent stem cells. The BRN3B-tdTomato construct was transfected into stem cells with reporter BRN3B-tdTomato. Cells were electroporated at 1,300V for 20 ms. After transfection, genotyping and sequence verification followed to select for the cells that had stably integrated the genetic cargo.

Generation of CtBP2-tdTomato integrated pluripotent stem cells. The CtBP2-tdTomato construct was transfected into stem cells. Cells were electroporated at 1,300V for 20 ms. After transfection, genotyping and sequence verification followed to select for the cells that had stably integrated the genetic cargo.

Generation of Tet-inducible NAIB integrated pluripotent stem cells. The NAIB construct was transfected into stem cells with reporter BRN3A-Neon as well as into stem cells with dual reporter BRN3A-Neon and BRN3B-tdTomato. Additionally, the pY026 plasmid, which expresses huAsCpf1 and crRNA, was co-transfected into the cells. Cells were electroporated at 1,300V for 20 ms. After transfection, cells were maintained in mTeSR with zeocin (200 ug/ml) for three weeks to select for the cells that had stably integrated the genetic cargo.

Direct conversion by activation of Tet-inducible expression of NAIB. Stem cells were pre-treated with LDN (1:10,000) and doxy (1:1000). PLO plates were set and placed in a hypoxia for 24 hours. The next day, PLO was aspirated, and the wells were washed three times with water and let dry in the hood for one hour. Matrigel was added in the wells and the plate was placed in the incubator for at least three hours. Cells were passaged to single cell density using Accutase for 12 minutes at 37°C. Following this, cells were quenched with mTeSR and 5μM blebbistatin, pelleted at 80 x g for 5 minutes, resuspended in neural induction medium (NIM) with 5μM blebbistatin, 1μM of doxycycline, 1:10,000 LDN, and 1:100 Cell One. NIM consists of DMEM/F12, HEPES (#11330032; Life technologies), N2 supplement (#17502048; Life technologies), Non-essential amino acids (#11140050; Life technologies), and Gluta-MAX (#25030081; Life technologies). These cells were then plated at about 54,000 cells per well on a 6 well plate. Every two days, cells were feed with 1 mL of prewarmed NIM + doxycycline (1:500) + Cell One (1:100). At days -1, 4, 5 and 6, cells were imaged in bright field at 10x and 20x fields of view to visualize neurite

outgrowth. Fluorescence imaging using an ImageXpress microscope was carried out after six days to measure fluorescence intensity of BRN3A-Neon. The FITC filter was used to visualize the Neon channel.

Directed differentiation into retinal organoids. Optic vesicles were generated as previously described (Wahlin et al. 2017) with minor modifications. Cell culture medium used for differentiation was as follows: BE6.2-NIM (B27 + E6 at 2X concentration) (neural induction medium) consists of DMEM (#11965; Invitrogen) supplemented with 1% B27 vitamin A (-) (#12587010; Invitrogen) and 2X E6 supplement (38.8 mg/L insulin (#11376497001; Roche), +128mg/L L-ascorbic acid (#A8960; Sigma), 28µg/L selenium (#S5261; Sigma), 21.4 mg/L transferrin (#T0665; Sigma) and 38.8 mg/L NaHCO3). LTR (Long-Term Retina) medium was a 3:1 mix of DMEM:F12 (#11965, #11765; Invitrogen) supplemented with 1% B27 (#17504044; Invitrogen), 10% heat inactivated qualified-grade FBS (#16140071; Invitrogen), 1mM pyruvate (#11360; Invitrogen), 1xNEAA (#11140; Invitrogen), 1xGlutamax (#35050061; Invitrogen) and 1mM taurine (#T-8691; Sigma). For optic vesicle induction, PSCs maintained in mTeSR1 were used to initiate serum-free embryoid body forced aggregates. Stem cells were passaged with a longer Accutase incubation for 12 minutes and 1,000 cells in 50µl of mTeSR1+B were seeded per well into polystyrene 96-well U-bottom plates (#650180; Greiner). Aggregates were transitioned to BE6.2 medium by adding 50µl+2% MG on day 1 and 1% MG each day thereafter. On days 4-8, a 50% medium exchange (100 µl) was performed daily and every other day thereafter. Medium contained 1% (v/v) MG and 3µM of IWR-1e (a WNT inhibitor and AXIN2 stabilizer; #681669; EMD Millipore) from days 1-6. For long term maintenance, vesicles were transferred at day 10 to 15ml conical tubes, rinsed 3 times in HBSS, and resuspended in BE6.2+300nM Smoothened agonist (SAG; #566660; EMD Millipore) from days 10-12 to enhance retinal induction then

LTR+SAG from days 12-18. For experiments longer than 16 days, we used sharpened tungsten needles to excise optic vesicles to prevent overgrowth and necrosis. Excision was typically carried out from days 10-12. To increase survival and differentiation, 500nM all-trans retinoic acid (ATRA; #R2625; Sigma) was added to LTR medium from day 20.

FIGURES

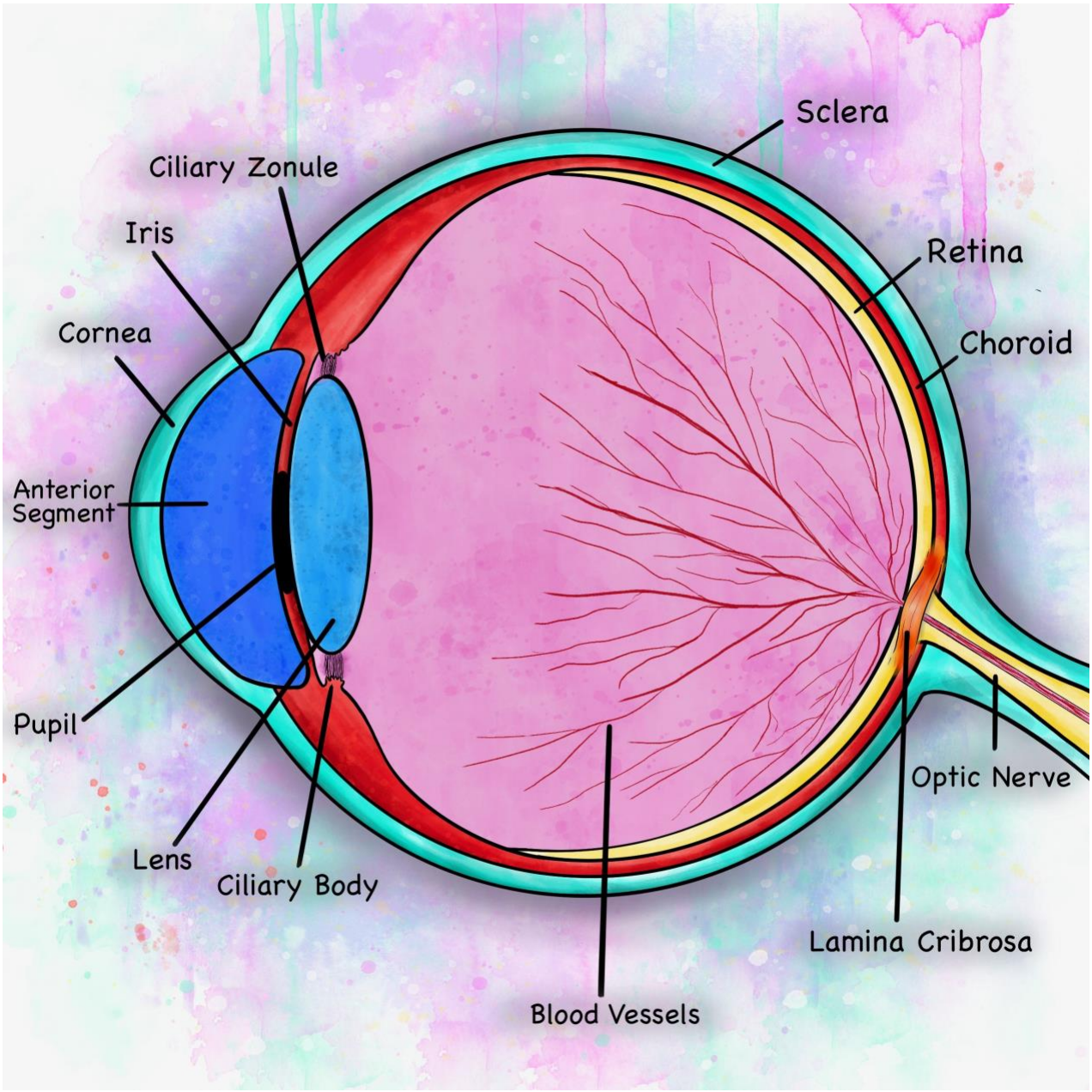

Figure 1: Architecture of the eye, including the optic nerve and lamina cribrosa. Adapted from SQ Online Illustration by Sara Kian. The retina is the innermost layer of the eye and receives light that has been focused by the lens. It then converts light into neural signals that get sent through the optic nerve and eventually to the brain, where visual perception occurs. The lamina cribrosa is a mesh-like structure that is in the hole of the sclera where retinal ganglion cell axons forming the optic nerve leave the eye. Displacement of the lamina cribrosa due to changes in the intraocular pressure results in the pinching of the nerve fibers and blood vessels in the optic nerve. This is one of the main causes of nerve damage in glaucoma.

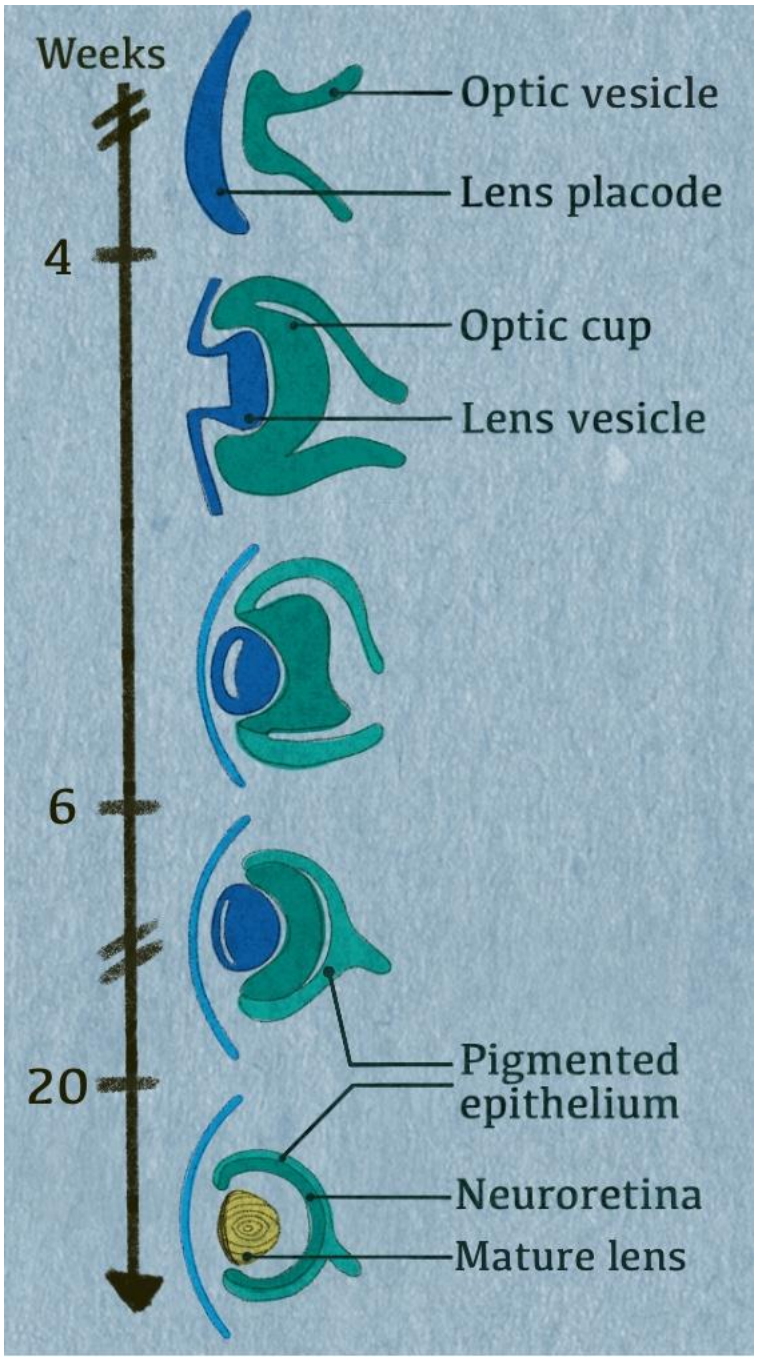

Figure 2: Human eye development. Illustrated by Sara Kian and adapted from Human eye conditions: insights from the fly eye by Gaspar et al., 2018. During week 4 of human embryogenesis, the optic vesicles evaginate from the forebrain neuroectoderm which causes the adjacent ectoderm to form the lens placode. The optic vesicle then invaginates upon itself sometime between weeks 4 and 6 and forms the optic cup that encompasses the invaginating lens vesicle. Between weeks 6 and 20, the optic cup differentiates into the neuroretina and the pigmented epithelium at the same time as the lens vesicle thickens and differentiates into the crystalline lens. Within the neuroretina, the neural cells move from the center to the periphery of the optic disc, which become the regions replete with photoreceptors in the adult retina.

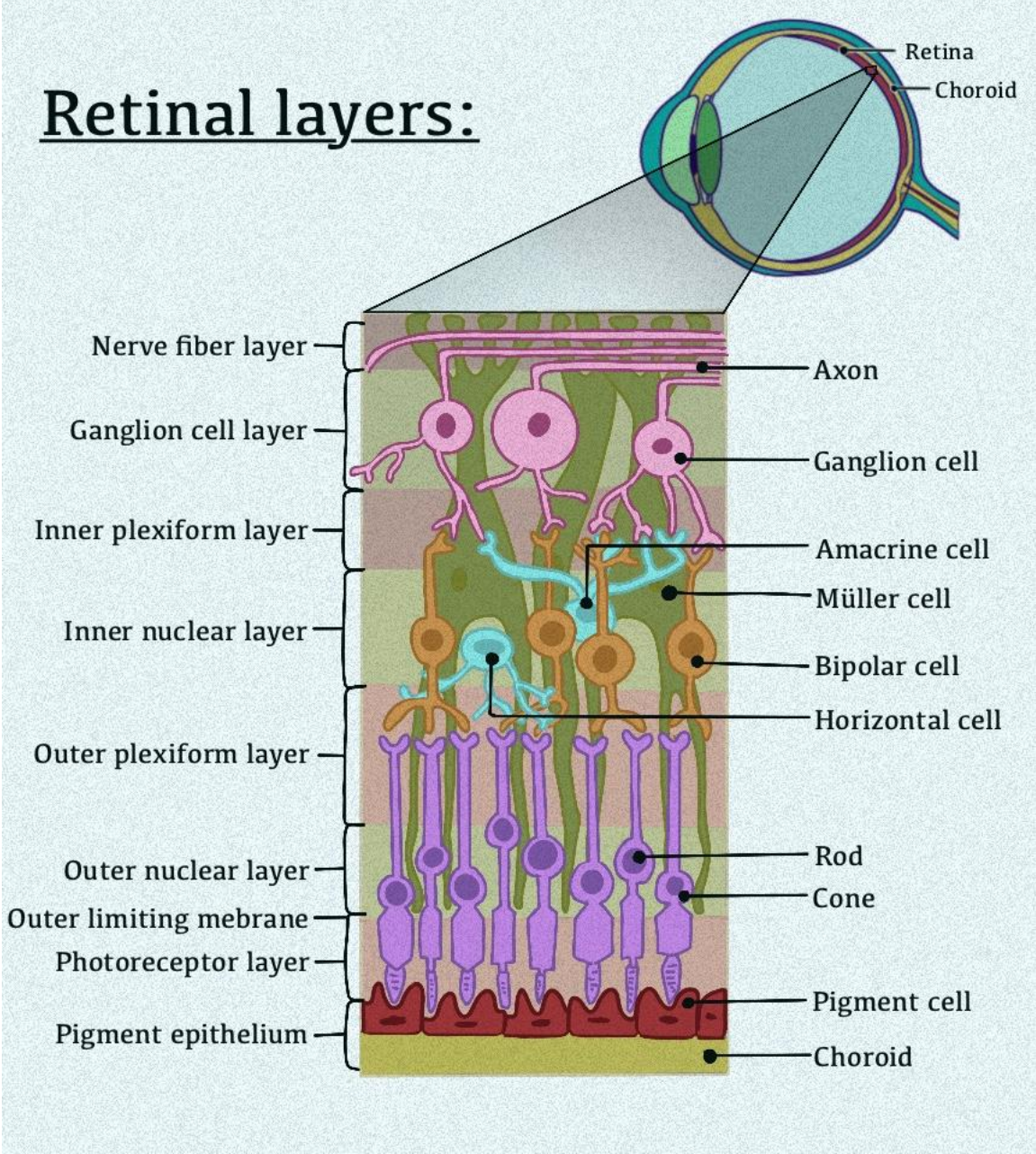

Figure 3: Structural organization of the retina. Illustrated by Sara Kian. The retina consists of five main cell types: retinal ganglion cells, photoreceptors (rods and cones), horizontal cells, amacrine cells, and bipolar cells. There are also three types of glial cells, including microglia, astrocytes, and Müller glia. The outer nuclear layer (ONL) of the retina is composed of the photoreceptors (rods and cones). Their axons elongate towards the outer plexiform layer (OPL), where synapstic triad is formed with bipolar and horizontal cells. Bipolar cells synapse with RGCs in the inner plexiform layer (IPL) that send light signals towards the brain. Using lateral inhibition, amacrine and horizontal cells modulate these light signals to allow for a high degree of visual acuity.

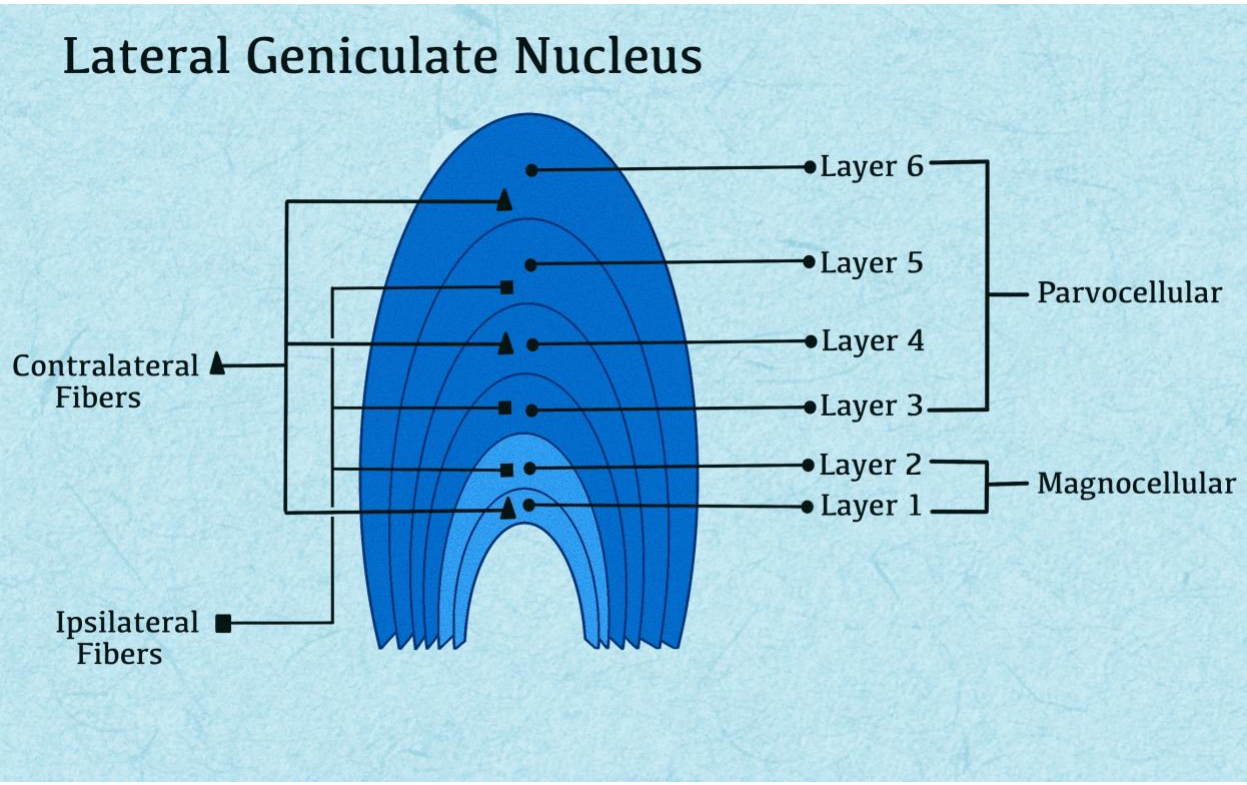

Figure 4: Structural organization of the lateral geniculate nucleus. Illustrated by Sara Kian. Most RGCs project to the lateral geniculate nucleus (LGN) in the dorsal thalamus. Midget cells project to the parvocellular layers of the LGN, parasol cells project to the magnocellular layers of the LGN and bistratified cells project to the koniocellular layers of the LGN.

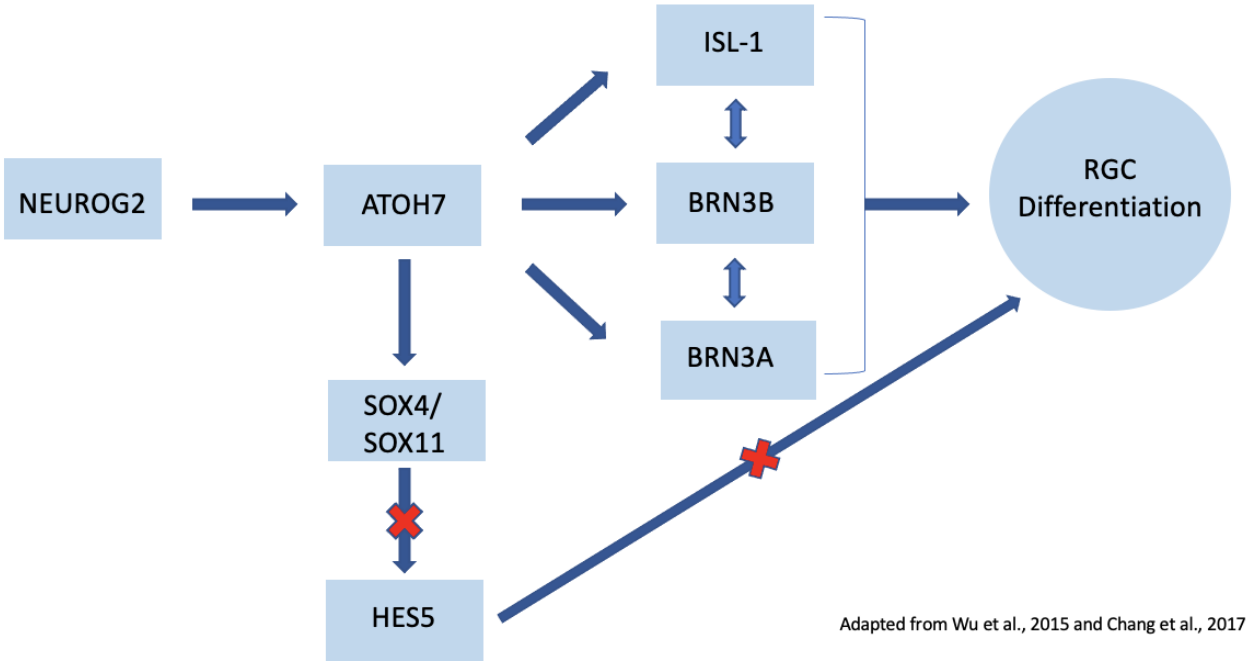

Figure 5: Relationship between transcription factors and their role in RGC differentiation. NEUROG2 induces neurogenesis and activates ATOH7, a major transcription factor for RGC commitment. ATOH7 activates ISL-1, BRN3B, and BRN3A, all of which drive the retinal progenitor cell to an RGC fate. ATOH7 also activates SOX4/SOX11, which induce RGC differentiation by inhibiting HES5, a transcription factor that inhibits RGC differentiation.

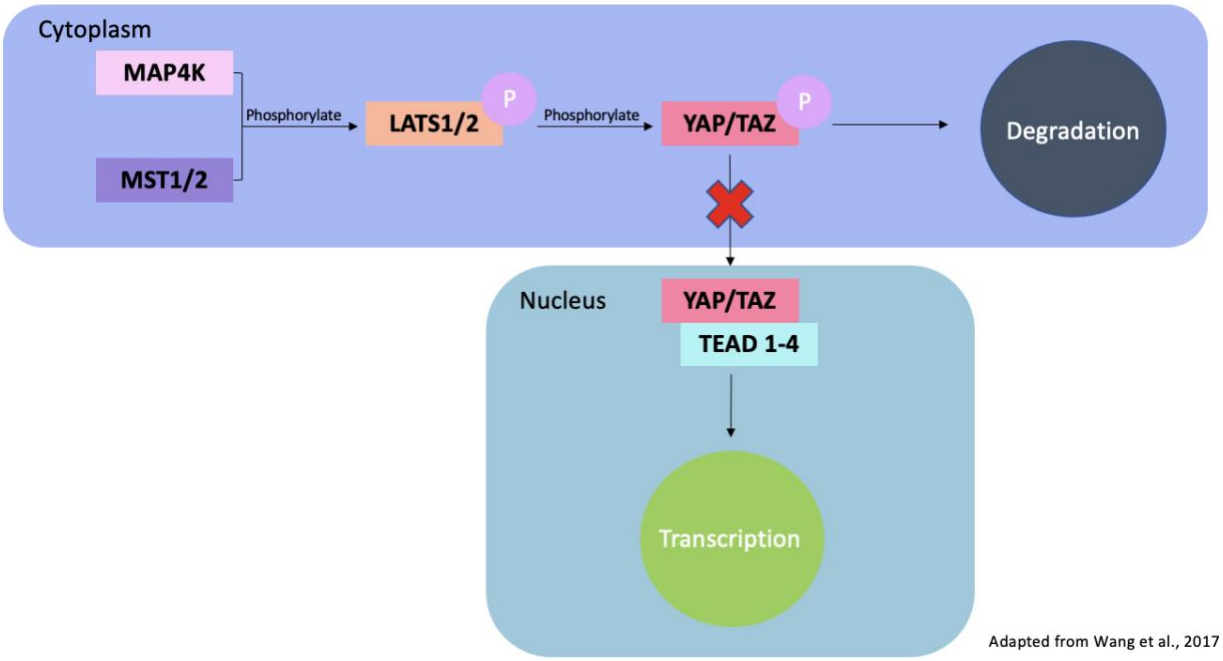

Figure 6: The mammalian Hippo signaling pathway. MST1/2 and MAP4K phosphorylate LATS1/2 which phosphorylates YAP/TAZ. The phosphorylation of YAP/TAZ leads to the inactivation and degradation of these two proteins. When the Hippo signaling pathway is inhibited, YAP/TAZ are unphosphorylated and move into the nucleus, where they form a complex with TEAD 1-4 and assist in the process of transcription. This pathway is involved in human eye development by differentiating the optic neuroepithelium, generating RPE cells, and interacting with other pathways such as Wnt/β-catenin, BMP and Notch pathways.

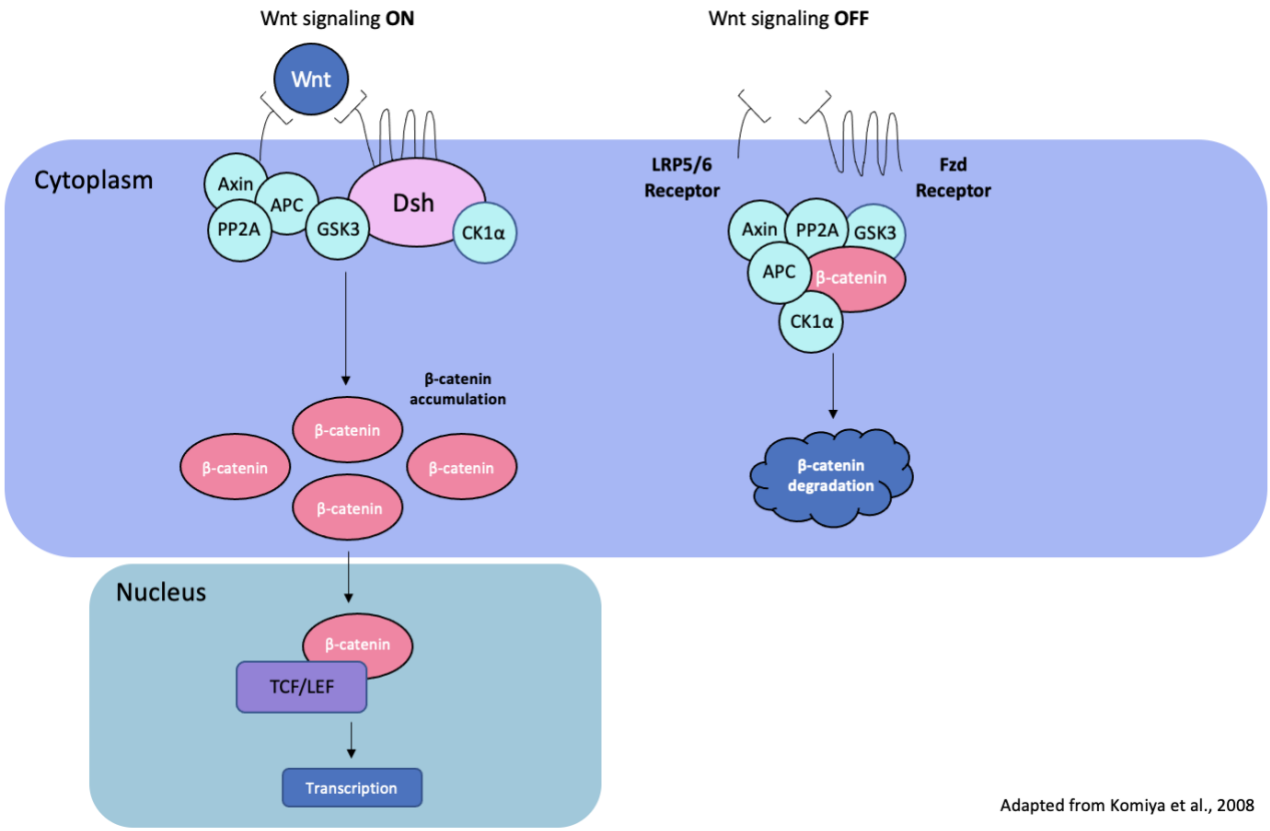

Figure 7: The canonical Wnt signaling pathway. When the Wnt ligand is not present, a β-catenin destruction complex consisting of Axin, PP2A, APC, CK1α, and GSK3 forms. This complex binds to and degrades β-catenin. When the Wnt ligand is bound to the Fzd and LRP5/6 receptors, Axin binds to the LRP5/6 receptor, which inactivates the β-catenin destruction complex. CK1α and Axin also activate the phosphoprotein Dsh, which downregulates GSK3 activity. This downregulation activates a signaling cascade that results in the accumulation of β-catenin in the cytoplasm. β-catenin then translocates into the nucleus, where it makes a complex with TCF/LEF to assist in transcription.

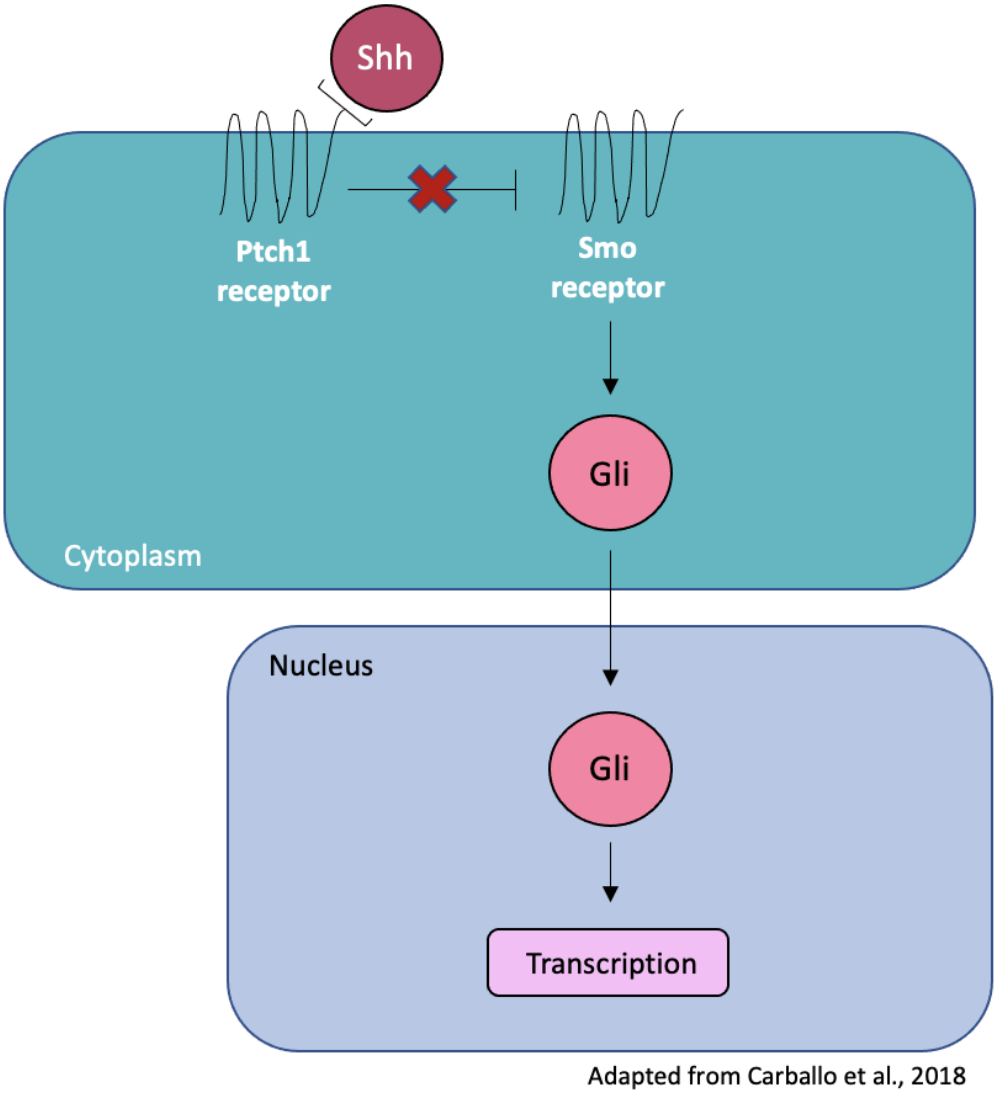

Figure 8: The canonical Shh signaling pathway. Shh binds to and inactivates the Ptch1 receptor. Ptch1 typically inactivates Smo and thus, when Ptch1 is inactivated, Smo gets upregulated. Smo then activates many signaling pathways that lead into the accumulation of the Gli protein, which translocates into the nucleus assisting in the process of transcription.

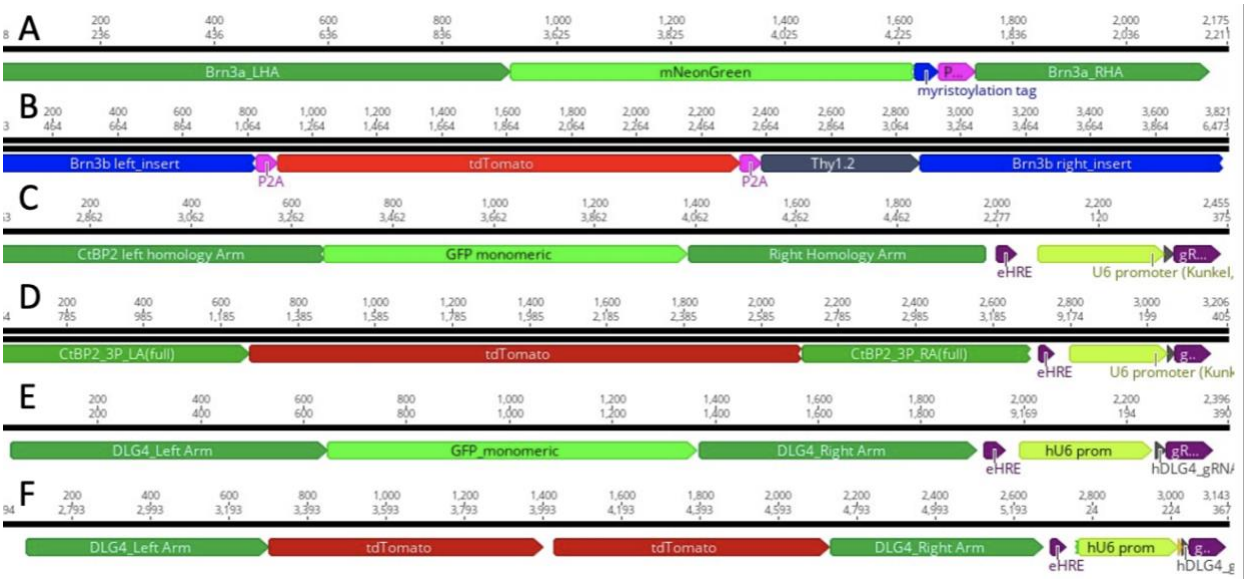

Figure 9: Plasmid maps of fluorescent reporters. The BRN3A-Neon (A) and BRN3B-tdTomato (B) donor plasmids have left and right homology arms, p2A sequences for polycistronic expression as well as mNeonGreen or tdTomato fluorescent markers respectively. (A) BRN3A-Neon also contains a myristoylation tag, while (B) BRN3B-tdTomato contains a Thy1.2 sequence, both of which localize the fluorescent proteins into the membrane of the cell. The CtBP2-GFP (C) and CtBP2-tdTomato (D) donor plasmids have left and right homology arms, eHRE for transfection efficiency purposes, as well as a hU6 promoter that expresses the gRNA and gRNA scaffold V3. They also have GFP or tdTomato fluorescent markers respectively. The DLG4-GFP (E) and DLG4-tdTomato (F) plasmids have left and right homology arms, eHRE for transfection efficiency purposes, GFP or tdTomato fluorescent markers respectively as well as a hU6 promoter that expresses the gRNA and gRNA scaffold V3.

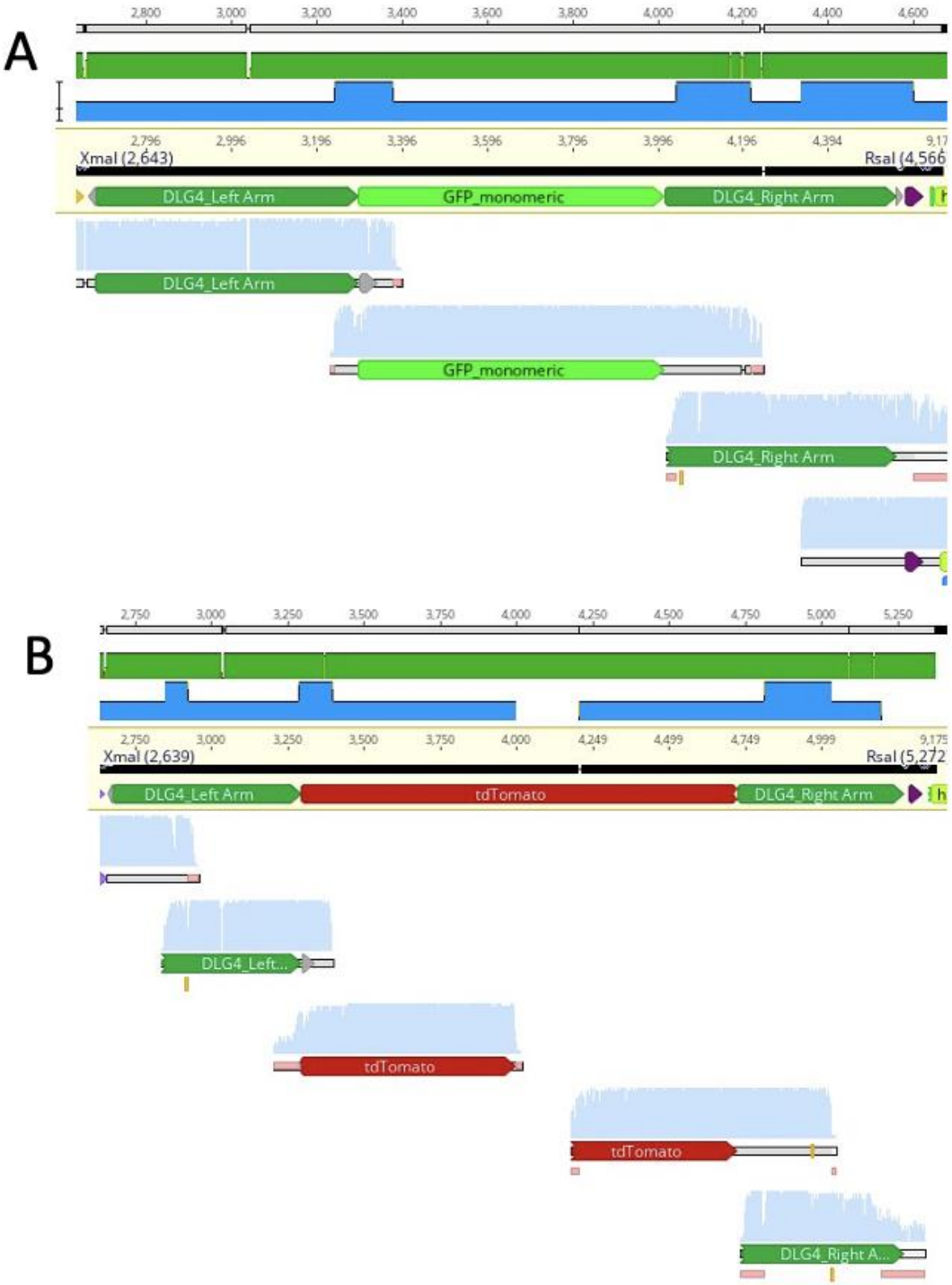

Figure 10: **Sanger sequencing verification of DLG4-GFP and DLG4-tdTomato plasmids.** A contig assembly was generated using the Geneious Prime package (Biomatters) and aligned sequences were graphically represented to show overlap coverage between Sanger sequenced files and the expected DLG4-GFP (A) and DLG4-tdTomato (B) plasmids. Overlapping sequencing reactions were performed in a redundant fashion to ensure high quality reads and full coverage of newly synthesized gene fragments.

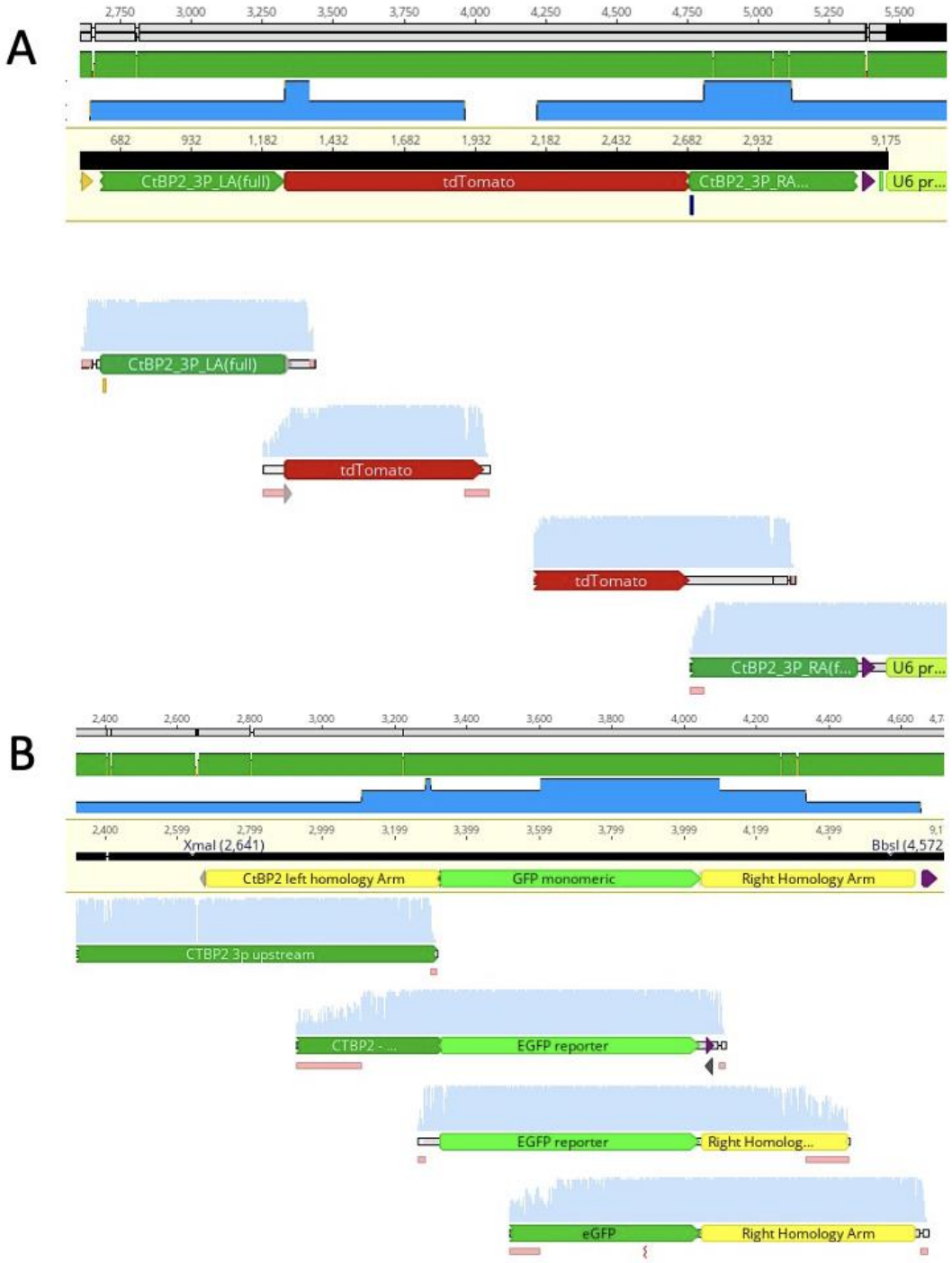

Figure 11: **Sanger sequencing verification of CtBP2-tdTomato, and CtBP2-GFP plasmids.** A contig assembly was generated using the Geneious software package (Biomatters) and aligned sequences were graphically represented to show overlap coverage between Sanger sequenced files and the expected CtBP2-tdTomato (A) and CtBP2-GFP (B) plasmids. Overlapping sequencing reactions were performed in a redundant fashion to ensure high quality reads and full coverage of newly synthesized gene fragments.

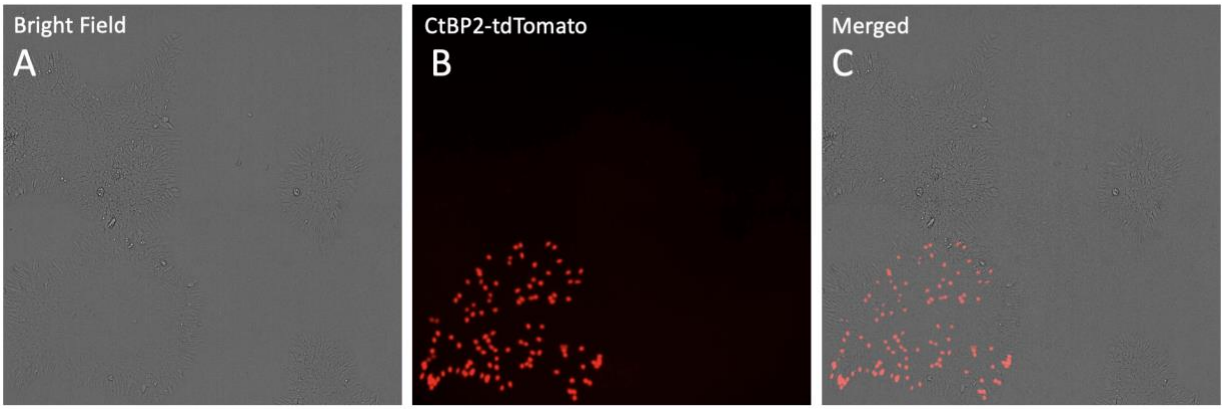

Figure 12: Expression of CtBP2-tdTomato in transfected human pluripotent stem cells. (A) Human pluripotent stem cells that have been transfected with the CtBP2-tdTomato plasmid were imaged by brightfield microscopy. (B) While CtBP2-tdTomato can label either synaptic proteins or the nucleus, in stem cells, it is expressed only in the nucleus. Stable integration of tdTomato was confirmed by fluorescent microscopy which showed clear nuclear localization of CtBP2-tdTomato within the nucleus. (C) Merging bright-field and CtBP2-tdTomato channels illustrating the stem cell morphology illustrated clonal expansion of stably integrated cells.

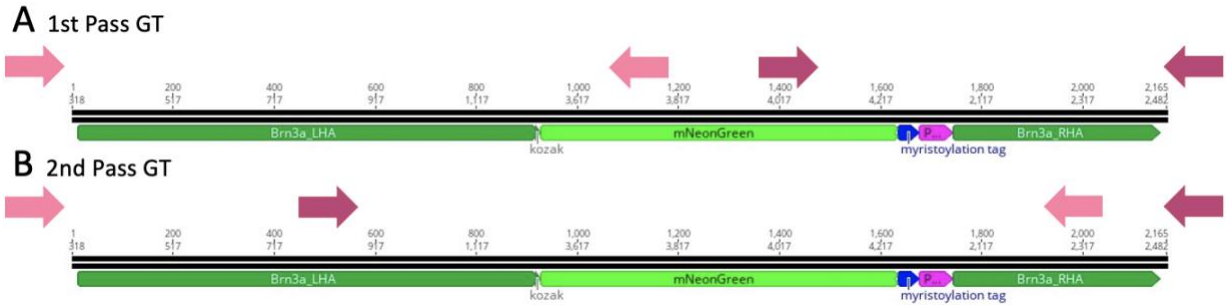

Figure 13: Oligonucleotide design for genotyping. (A) First pass genotyping is used to determine whether the insert was stably integrated into the genome. One oligonucleotide is designed outside of a homology arm while the other is designed within the desired insert. Amplification only occurs if the insert is successfully integrated into the genome. The pink and magenta arrows are two possible oligonucleotide pairs. (B) Second pass genotyping is used to discriminate between the heterozygous or homozygous integration of the insert into the genome. The first oligonucleotide is chosen outside of a homology arm, while the second oligonucleotide is chosen inside the other homology arm. The pink and magenta arrows are two possible oligonucleotide pairs.

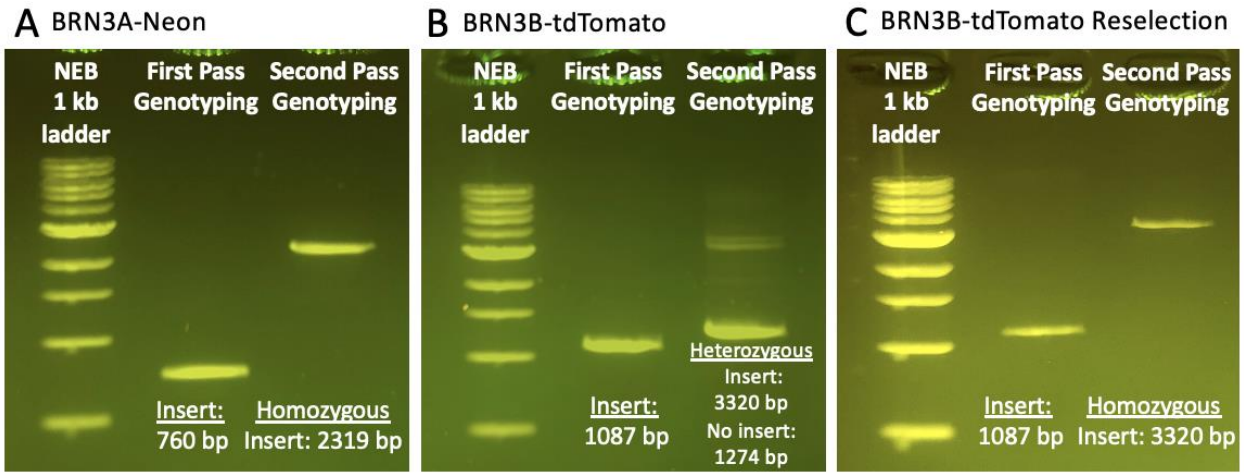

Figure 14. **Genotyping verification of Dual Reporter BRN3A-Neon and BRN3B-tdTomato.** Through first and second pass genotyping, the dual RGC reporter BRN3A-Neon and BRN3B-tdTomato cell line was verified. (A) For first pass genotyping of BRN3A-Neon, a band at 760 base pairs (bp) was clearly visible. This band signified the successful insertion of Neon-Myristoylation Tag-p2A into the BRN3A gene. For second pass genotyping, a band at 2319 bp was clearly visible, which signified the homozygous insertion of Neon-Myristoylation Tag-p2A into the BRN3A gene. (B) For first pass genotyping of BRN3B-tdTomato, a band at 1087 bp was clearly visible. This band signified the successful insertion of p2A-tdTomato-p2A-Thy1.2 into the BRN3B gene. For second pass genotyping, bands at 3320 bp and 1274 were clearly visible. The band at 3320 bp verified the integration of the fluorescent protein into the genome, while the band at 1274 bp signified the lack of insert in the genome. Because both bands are visible, at first glance, we assumed that there was a heterozygous insertion of p2A-tdTomato-p2A-Thy1.2 into the BRN3B gene. However, the intensity of the bands differed, meaning that this could have been a mixed population. (C) After colony-picking and genotyping once more, this hypothesis was confirmed. A colony in this mixed population showed a single band at 3320 bp for second pass genotyping, which confirmed the homozygous integration of p2A-tdTomato-p2A-Thy1.2 into the BRN3B gene

Figure 15: Sanger sequencing verification of the homozygous insertion of Neon-Myristoylation Tag-P2A into the BRN3A gene. A contig assembly was generated using the Geneious software package (Biomatters) and aligned sequences were graphically represented to show overlap coverage between Sanger sequenced files and the expected BRN3A-Neon-Myristoylation Tag-P2A sequence. Overlapping sequencing reactions were performed in a redundant fashion to ensure high quality reads and full coverage of newly synthesized gene fragments.

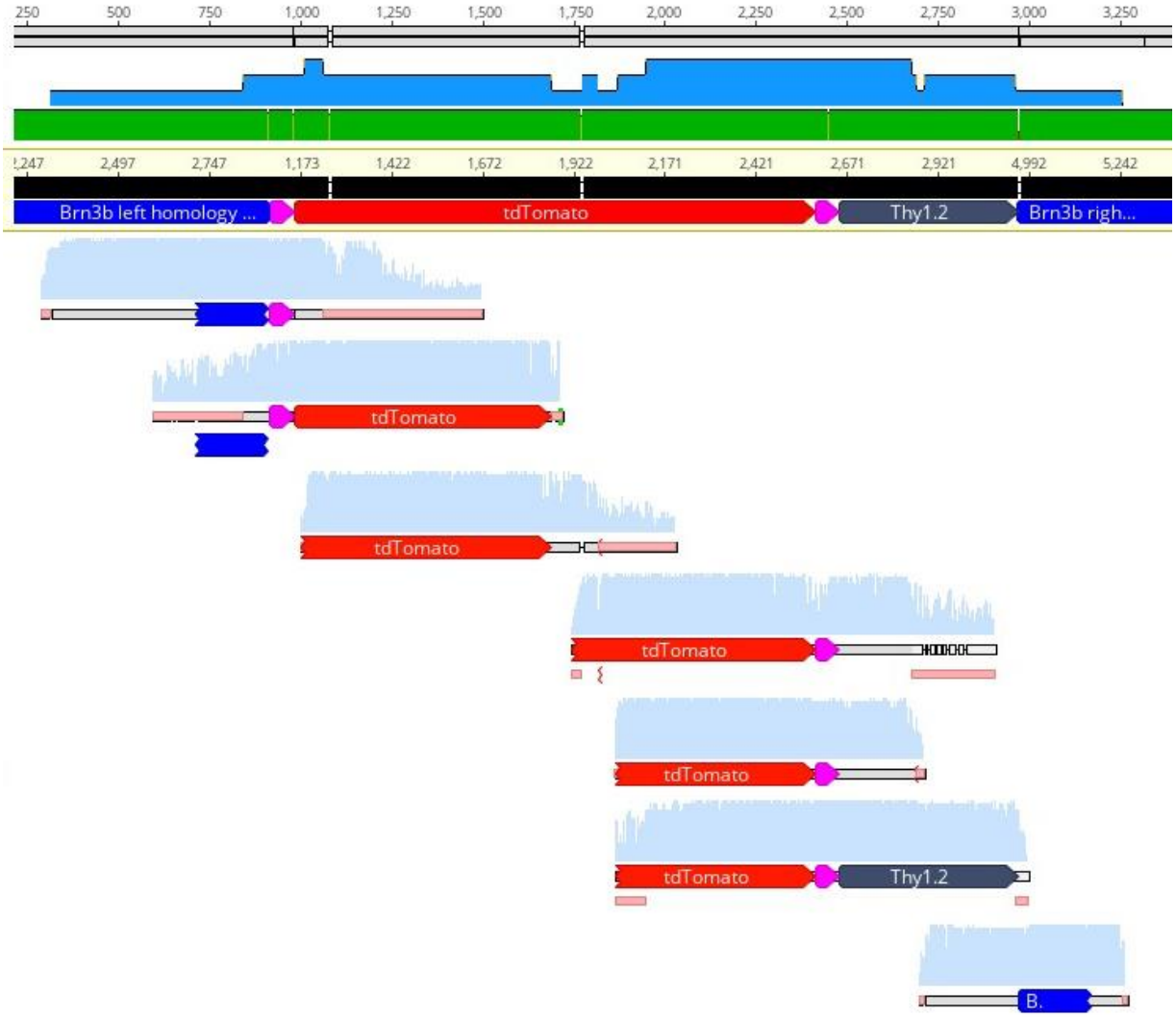

Figure 16: Sanger sequencing verification of the homozygous insertion of P2A-tdTomato-P2A-Thy1.2 into the BRN3B gene. A contig assembly was generated using the Geneious software package (Biomatters) and aligned sequences were graphically represented to show overlap coverage between Sanger sequenced files and the expected BRN3B-P2A-tdTomato-P2A-Thy1.2 sequence. Overlapping sequencing reactions were performed in a redundant fashion to ensure high quality reads and full coverage of newly synthesized gene fragments.

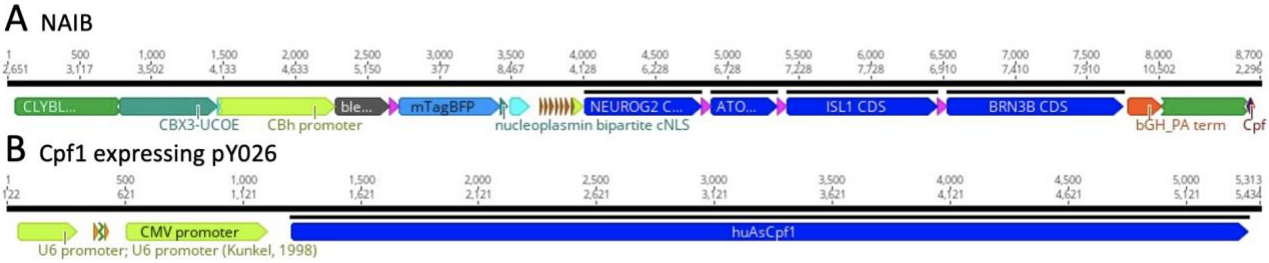

Figure 17: Plasmid constructs for NAIB and Cpf1 expressing pY026. (A) The NAIB plasmid construct contained four RGC expressed genes (NEUROG2, ATOH7, ISL1, and BRN3B), each separated by a P2A sequence enabling polycistronic expression of genes via ribosome skipping. The NAIB cassette is controlled by a third-generation tetracycline (TET) activated response element (3G-TRE) and a constitutively expressed reverse tetracycline trans-activating sequence (rtTA). Under a chicken beta-actin hybrid (Cbh) promoter, a constitutively active TagBFP2 is included in the plasmid construct to verify gene integration. TagBFP is also co-expressed with a zeocin selectable marker to remove unmodified cells and obtain a pure population of NAIB integrated cells. (B) The Cpf1 expressing pY026 plasmid was also used. This plasmid co-expresses a Cpf1 enzyme and a CLYBL targeting guide sequence allowing us to stably insert genetic cargo into pluripotent stem cells.

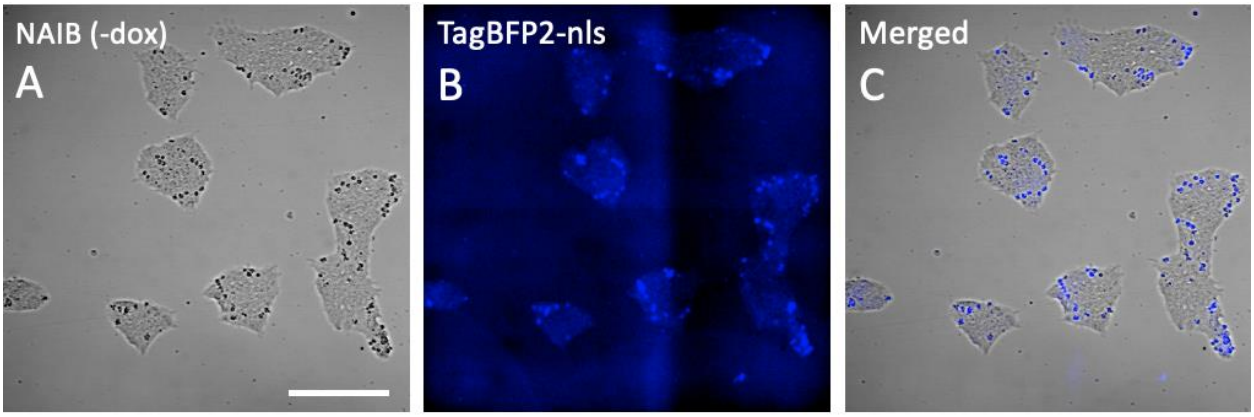

Figure 18: Verification of the NAIB integrated BRN3A-Neon cells via the mTagBFP2 signal. (A) Bright field images of NAIB integrated BRN3A-Neon cells. (B) TagBFP2-nls was used to mark the NAIB integrated cells. Therefore, we were able to verify the stable integration of NAIB by fluorescent microscopy. Colonies that express TagBFP2-nls is clearly visible. (C) Merged bright-field and TagBFP2-nls channels illustrating the stem cell morphology aligning with the TagBFP2-nls signal. Scale bars = 250 μm.

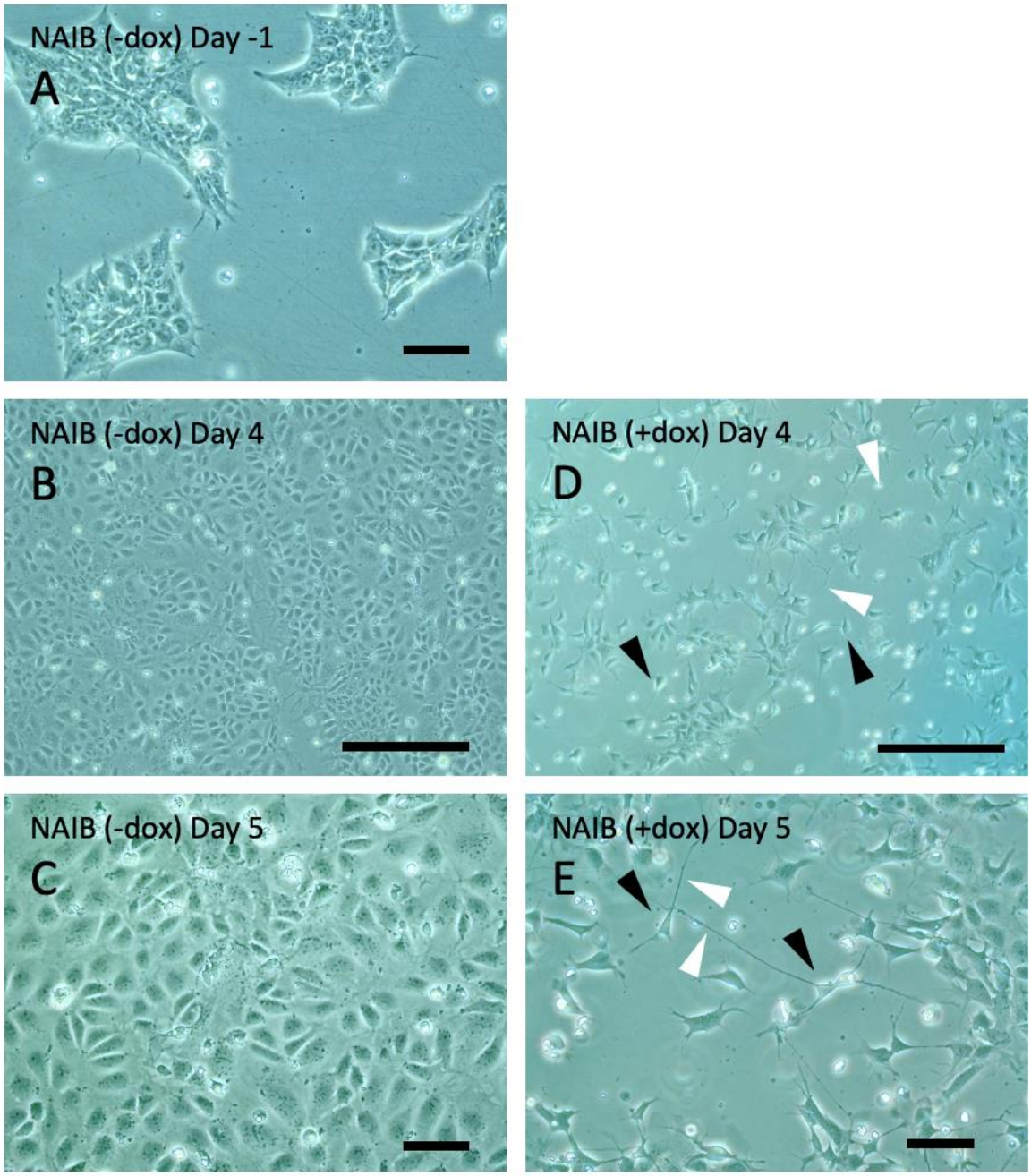

Figure 19: Comparing the morphology of NAIB integrated cells with and without doxycycline. (A) BRN3A-Neon NAIB integrated IMR90 hiPSCs -1 days before doxycycline treatment. Cells were enriched by zeocin selection but not treated with doxycycline (B-C) Control BRN3A-Neon NAIB integrated IMR90 hiPSCs treated with Cell Culture One and LDN, but not doxycycline after 4 days (B) and 5 days (C). No neuronal morphology was observed. (D-E) BRN3A-Neon NAIB integrated IMR90 hiPSCs treated with Cell Culture One, LDN, and doxycycline after 4 days (D) and 5 days (E). Neuronal morphology was observed. Images were taken using the Leica microscope. Scale bars = 300 μm

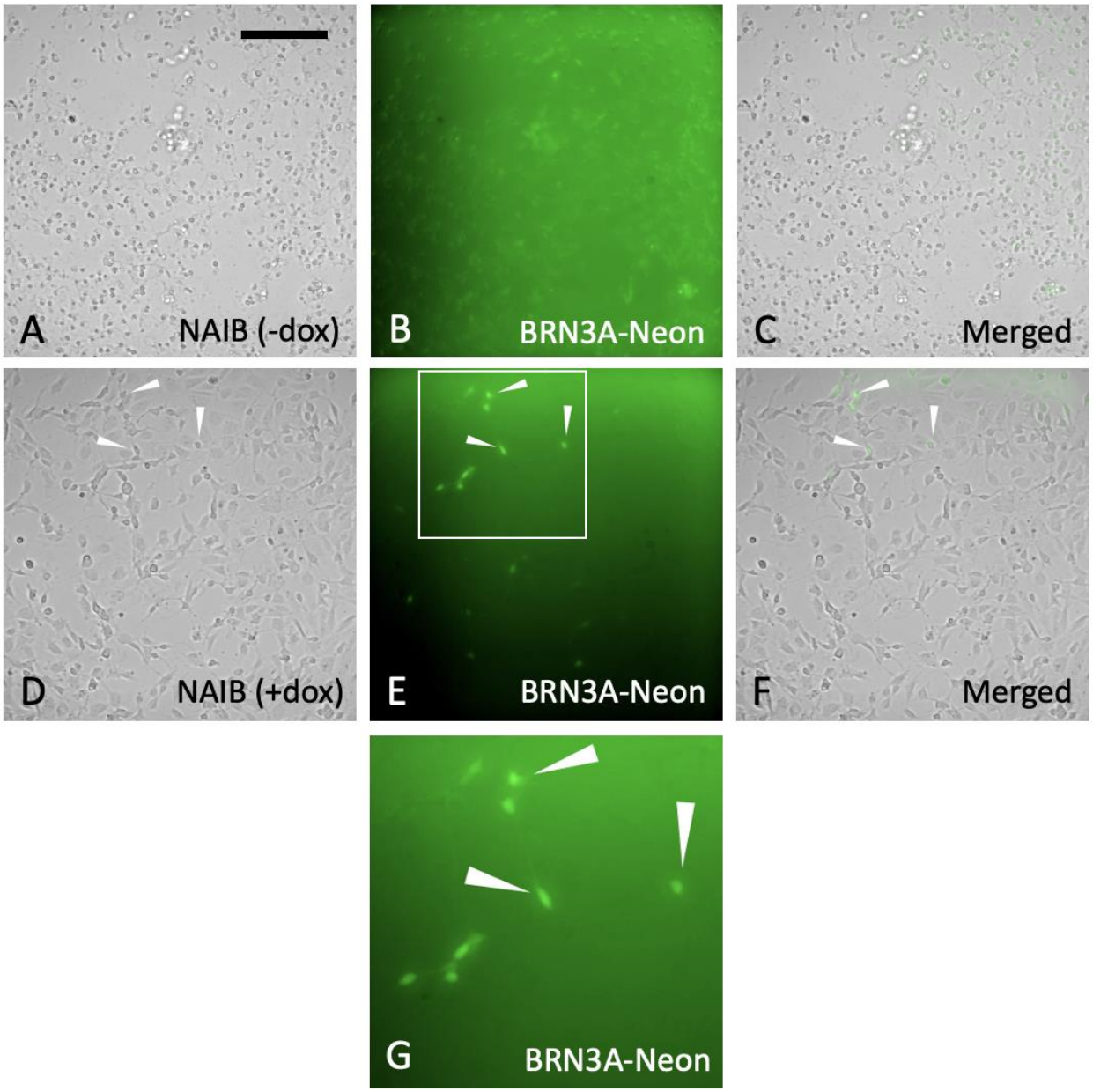

Figure 20: BRN3A-mNeonGreen expression in NAIB integrated cells. (A-C) Control NAIB integrated cells were not treated with doxycycline and (B) did not show the BRN3A-Neon signal, suggesting that BRN3A was not expressed. (D-G) After six days of doxycycline treatment, NAIB integrated cells were visualized. (E and G) Under the fluorescent microscope, some of the hPSC-induced RGCs showed the BRN3A-Neon signal, indicating that a portion of the neurons expressed BRN3A. Scale bars = 250 μm

TABLES

Table 1: Oligonucleotides for construct modifications.

a. CtBP2-GFP

Gene Name	NAME	Sequence
gRNA scaffold V3	C2273_CtBP2_guideV3_R C1548 Cas9DumScafv3swap_F	CTGTTTCCAGCTTAGCTCTTAAACGAAGGTAATCACTCAGATACGGTGTTTCGTCCTTTCCACAAGATATATAAAGCCAAGA GTTTAAGAGCTAAGCTGGAAACAGCATAGCAAGTTTAAATAAGGCTAGTCCGTTA
eHRE	C248_eHRE_rev C1489 2xHRE insert F	TTCACATACACACGTACACGCACACACATACATCCGCGCAAAGCTTGGTACCAAA GGATGTATGTGTGTGCGTGTACGTGTGTATGTGAAGATACCGCCTAGGCGCCTAGGGAATTCGCGGCCG
GFP fix	C2310_CtBP2_GFPfix_R C2309_CTBP2_GFPfix_F	GCTCACCATTGCTCGTTGGGGTGCTCTCGATTGT CCCAACGAGCAATGGTGAGCAAGGGCGAGGAGCTGTTCACCGGGGTGGTGCCCATC

b. CtBP2-tdTomato

Gene Name	NAME	Sequence
gRNA scaffold V3	C2272_CtBP2-gRNAV3swapR C1548 Cas9DumScafv3swap_F:	GTTTCCAGCTTAGCTCTTAAACGAAGGTAATCACTCAGATAC GTTTAAGAGCTAAGCTGGAAACAGCATAGCAAGTTTAAATAAGGCTAGTCCGTTA
eHRE	C248_eHRE_rev C1489 2xHRE insert F	TTCACATACACACGTACACGCACACACATACATCCGCGCAAAGCTTGGTACCAAA GGATGTATGTGTGTGCGTGTACGTGTGTATGTGAAGATACCGCCTAGGCGCCTAGGGAATTCGCGGCCG

Table 1: Continued.

c. DLG4-GFP

Gene Name	NAME	Sequence
gRNA scaffold V3	C2271_DLG4_V3swap C1548 Cas9DumScafv3swap_F:	TTTCCAGCTTAGCTCTTAAACAGAGAGACTCTGATTCCTGCGGTGTTTCGTCCTT GTTTAAGAGCTAAGCTGGAAACAGCATAGCAAGTTTAAATAAGGCTAGTCCGTTA
eHRE	C248_eHRE_rev C1489 2xHRE insert F	TTCACATACACACGTACACGCACACACATACATCCGCGCAAAGCTTGGTACCAAA GGATGTATGTGTGTGCGTGTACGTGTGTATGTGAAGATACCGCCTAGGCGCCTAGGGAATTCGCGGCCG

d. DLG4-tdTomato

Gene Name	NAME	Sequence
gRNA scaffold V3	C2271_DLG4_V3swap C1548 Cas9DumScafv3swap_F:	TTTCCAGCTTAGCTCTTAAACAGAGAGACTCTGATTCCTGCGGTGTTTCGTCCTT GTTTAAGAGCTAAGCTGGAAACAGCATAGCAAGTTTAAATAAGGCTAGTCCGTTA
eHRE	C248_eHRE_rev C1489 2xHRE insert F	TTCACATACACACGTACACGCACACACATACATCCGCGCAAAGCTTGGTACCAAA GGATGTATGTGTGTGCGTGTACGTGTGTATGTGAAGATACCGCCTAGGCGCCTAGGGAATTCGCGGCCG

Table 2: Oligonucleotides for genotyping.

a. BRN3A-Neon

Genotyping	**NAME**	**Sequence**
First Pass	G373_Brn3aGT_R1_Rev G219_Rhod_geno1303_Neon_F	AGAGGGAAAAGAAGAAATGGAAATGTAACTC TGCGCGGACCACCTACACCTT
Second Pass	G373_Brn3aGT_R1_Rev G405_Brn3aGT_1086_F	AGAGGGAAAAGAAGAAATGGAAATGTAACT CGGTGCCTGACACAGTTATATTCACAACAAC

b. BRN3B-tdTomato

Genotyping	**NAME**	**Sequence**
First Pass	G81 Tomato_GT_rev G22 Brn3b_2426NeonHomo_F	GCGCATGAACTCTTTGATGACCTCCT CCTGCTGAGCGTAATGTGTGCCTTCTACTT
Second Pass	G22 Brn3b_2426NeonHomo_F G23 Brn3b_2426NeonhomoR	CCTGCTGAGCGTAATGTGTGCCTTCTACTT CAAACAGCCATCTCCACACTTCCTCTGAA

REFERENCES

1. Adler R, Canto-Soler MV. Molecular mechanisms of optic vesicle development: Complexities, ambiguities and controversies. *Developmental Biology*. 2007;305(1):1-13. doi:10.1016/j.ydbio.2007.01.045

2. Albert S, Müller F, Fischer N, Biellmann D, Neumann C, Blader P, Strähle U. Cyclops independent floor plate differentiation in zebrafish embryos. *Developmental Dynamics*. 2003;226(1):59-66. doi:10.1002/dvdy.10211

3. Amin, N. D., & Paşca, S. P. (2018). Building Models of Brain Disorders with Three Dimensional Organoids. *Neuron*, *100*(2), 389 405. https://doi.org/10.1016/j.neuron.2018.10.007

4. Artero Castro, A., Rodríguez Jimenez, F. J., Jendelova, P., & Erceg, S. (2019). Deciphering retinal diseases through the generation of three dimensional stem cell-derived organoids: Concise Review. Stem cells (Dayton, Ohio), 37(12), 1496–1504. https://doi.org/10.1002/stem.3089

5. Badea, T. C., Cahill, H., Ecker, J., Hattar, S., & Nathans, J. (2009). Distinct roles of transcription factors brn3a and brn3b in controlling the development, morphology, and function of retinal ganglion cells. Neuron, 61(6), 852–864. https://doi.org/10.1016/j.neuron.2009.01.020

6. Beffagna G. Zebrafish as a Smart Model to Understand Regeneration After Heart Injury: How Fish Could Help Humans. *Front Cardiovasc Med*. 2019;6. doi:10.3389/fcvm.2019.00107

7. Bernardos, R. L., Barthel, L. K., Meyers, J. R., & Raymond, P. A. (2007). Late-stage neuronal progenitors in the retina are radial Müller glia that function as retinal stem cells. The Journal of neuroscience : the official journal of the Society for Neuroscience, 27(26), 7028–7040. https://doi.org/10.1523/JNEUROSCI.1624-07.2007

8. Brodie-Kommit, J., Clark, B. S., Shi, Q., Shiau, F., Kim, D. W., Langel, J., Sheely, C., Ruzycki, P. A., Fries, M., Javed, A., Cayouette, M., Schmidt, T., Badea, T., Glaser, T., Zhao, H., Singer, J., Blackshaw, S., & Hattar, S. (2021). Atoh7-independent specification of retinal ganglion cell identity. Science advances, 7(11), eabe4983. https://doi.org/10.1126/sciadv.abe4983

9. Bronner, M. E., & LeDouarin, N. M. (2012). Development and evolution of the neural crest: an overview. Developmental biology, 366(1), 2–9. https://doi.org/10.1016/j.ydbio.2011.12.042

10. Bucolo, C., Platania, C., Drago, F., Bonfiglio, V., Reibaldi, M., Avitabile, T., & Uva, M. (2018). Novel Therapeutics in Glaucoma Management. *Current neuropharmacology*, *16*(7), 978–992. https://doi.org/10.2174/1570159X15666170915142727

11. Burke J. M. (2008). Epithelial phenotype and the RPE: is the answer blowing in the Wnt?. Progress in retinal and eye research, 27(6), 579–595. https://doi.org/10.1016/j.preteyeres.2008.08.002

12. Capowski, E. E., Samimi, K., Mayerl, S. J., Phillips, M. J., Pinilla, I., Howden, S. E., Saha, J., Jansen, A. D., Edwards, K. L., Jager, L. D., Barlow, K., Valiauga, R., Erlichman, Z., Hagstrom, A., Sinha, D., Sluch, V. M., Chamling, X., Zack, D. J., Skala, M. C., & Gamm, D. M. (2019). Reproducibility and staging of 3D human retinal organoids across multiple pluripotent stem cell lines. Development (Cambridge, England), 146(1), dev171686. https://doi.org/10.1242/dev.171686

13. Carballo GB, Honorato JR, de Lopes GPF, Spohr TCL de S e. A highlight on Sonic hedgehog pathway. *Cell Commun Signal*. 2018;16(1):11. doi:10.1186/s12964-018-0220-7

14. Chang K-C, Hertz J. SoxC transcription factors in retinal development and regeneration. *Neural Regen Res*. 2017;12(7):1048. doi:10.4103/1673-5374.211178

15. Chen, G., Hou, Z., Gulbranson, D. R., & Thomson, J. A. (2010). Actin-myosin contractility is responsible for the reduced viability of dissociated human embryonic stem cells. *Cell stem cell*, *7*(2), 240–248. https://doi.org/10.1016/j.stem.2010.06.017

16. Clevers H. (2006). Wnt/beta-catenin signaling in development and disease. Cell, 127(3), 469–480. https://doi.org/10.1016/j.cell.2006.10.018

17. Clevers, H., Lancaster, M., & Takebe, T. (2017). Advances in Organoid Technology: Hans Clevers, Madeline Lancaster, and Takanori Takebe. *Cell Stem Cell*. Retrieved from https://www.cell.com/cell-stem-cell/comments/S1934-5909(17)30179-0

18. Costamagna D, Mommaerts H, Sampaolesi M, Tylzanowski P. Noggin inactivation affects the number and differentiation potential of muscle progenitor cells in vivo. *Scientific Reports*. 2016;6(1):31949. doi:10.1038/srep31949

19. CRISPR Guide. (n.d.). Retrieved April 17, 2021, from https://www.addgene.org/guides/crispr/?edit_off&gclid=CjwKCAjwjuqDBhAGEiwAdX2cj4E-bJ8ad8xxnzcW3ehGNrVdEwO9qRX0-t8On3vQaRZDlB4jku-2OBoCGxoQAvD_BwE

20. Cvekl, A., & Wang, W. L. (2009). Retinoic acid signaling in mammalian eye development. Experimental eye research, 89(3), 280–291. https://doi.org/10.1016/j.exer.2009.04.012

21. Daniels RW, Rossano AJ, Macleod GT, Ganetzky B. Expression of Multiple Transgenes from a Single Construct Using Viral 2A Peptides in Drosophila. McCabe BD, ed. PLoS ONE. 2014;9(6):e100637. doi:10.1371/journal.pone.0100637

22. Dhande, O. S., Stafford, B. K., Lim, J. A., & Huberman, A. D. (2015). Contributions of Retinal Ganglion Cells to Subcortical Visual Processing and Behaviors. Annual review of vision science, 1, 291–328. https://doi.org/10.1146/annurev-vision-082114-035502

23. DiStefano, T., Chen, H. Y., Panebianco, C., Kaya, K. D., Brooks, M. J., Gieser, L., Morgan, N. Y., Pohida, T., & Swaroop, A. (2018). Accelerated and Improved Differentiation of Retinal Organoids from Pluripotent Stem Cells in Rotating-Wall Vessel Bioreactors. Stem cell reports, 10(1), 300–313. https://doi.org/10.1016/j.stemcr.2017.11.001

24. Duester G. (2009). Keeping an eye on retinoic acid signaling during eye development. Chemico-biological interactions, 178(1-3), 178–181. https://doi.org/10.1016/j.cbi.2008.09.004

25. Eguizabal, C., Montserrat, N., Vassena, R., Barragan, M., Garreta, E., Garcia-Quevedo, L., Vidal, F., Giorgetti, A., Veiga, A., & Izpisua Belmonte, J. C. (2011). Complete meiosis from human induced pluripotent stem cells. Stem cells (Dayton, Ohio), 29(8), 1186–1195. https://doi.org/10.1002/stem.672

26. Eiraku, M., & Sasai, Y. (2011). Self-organizing optic-cup morphogenesis in three-dimensional culture. *Neuroscience Research, 71*. doi:10.1016/j.neures.2011.07.545

27. Eiraku, M., Takata, N., Ishibashi, H., Kawada, M., Sakakura, E., Okuda, S., . . . Sasai, Y. (2011). Self-organizing Optic-cup morphogenesis in Three-dimensional culture. Nature, 472(7341), 51-56. doi:10.1038/nature09941

28. El Agha, E., Kosanovic, D., Schermuly, R. T., & Bellusci, S. (2016). Role of fibroblast growth factors in organ regeneration and repair. Seminars in cell & developmental biology, 53, 76–84. https://doi.org/10.1016/j.semcdb.2015.10.009

29. Erkman, L., McEvilly, R. J., Luo, L., Ryan, A. K., Hooshmand, F., O'Connell, S. M., Keithley, E. M., Rapaport, D. H., Ryan, A. F., & Rosenfeld, M. G. (1996). Role of transcription factors Brn-3.1 and Brn-3.2 in auditory and visual system development. Nature, 381(6583), 603–606. https://doi.org/10.1038/381603a0

30. Fabre, P. J., Shimogori, T., & Charron, F. (2010). Segregation of ipsilateral retinal ganglion cell axons at the optic chiasm requires the Shh receptor Boc. The Journal of neuroscience : the official journal of the Society for Neuroscience, 30(1), 266–275. https://doi.org/10.1523/JNEUROSCI.3778-09.2010

31. Fligor, C. M., Langer, K. B., Sridhar, A., Ren, Y., Shields, P. K., Edler, M. C., Ohlemacher, S. K., Sluch, V. M., Zack, D. J., Zhang, C., Suter, D. M., & Meyer, J. S. (2018). Three-Dimensional Retinal Organoids Facilitate the Investigation of Retinal Ganglion Cell Development, Organization and Neurite Outgrowth from Human Pluripotent Stem Cells. *Scientific Reports*, *8*(1), 14520. https://doi.org/10.1038/s41598-018-32871-8

32. Fuhrmann, S. (2010). Eye morphogenesis and patterning of the Optic Vesicle. Current Topics in Developmental Biology, 61-84. doi:10.1016/b978-0-12-385044-7.00003-5

33. Gehring W. J. (2002). The genetic control of eye development and its implications for the evolution of the various eye-types. The International journal of developmental biology, 46(1), 65–73.

34. Giger FA, Houart C. The Birth of the Eye Vesicle: When Fate Decision Equals Morphogenesis. *Front Neurosci*. 2018;12:87. doi:10.3389/fnins.2018.00087

35. Gonzalez-Cordero, A., West, E. L., Pearson, R. A., Duran, Y., Carvalho, L. S., Chu, C. J., & Ali, R. R. (2013). Photoreceptor precursors derived from three-dimensional embryonic stem cell cultures integrate and mature within adult degenerate retina. *Nature Biotechnology, 31*(8), 741-747. doi:10.1038/nbt.2643

36. Guimarães, R., Landeira, B. S., Coelho, D. M., Golbert, D., Silveira, M. S., Linden, R., de Melo Reis, R. A., & Costa, M. R. (2018). Evidence of Müller Glia Conversion Into Retina Ganglion Cells Using Neurogenin2. Frontiers in cellular neuroscience, 12, 410. https://doi.org/10.3389/fncel.2018.00410

37. Haeryfar, S. M., & Hoskin, D. W. (2004). Thy-1: more than a mouse pan-T cell marker. Journal of immunology (Baltimore, Md. : 1950), 173(6), 3581–3588. https://doi.org/10.4049/jimmunol.173.6.3581

38. Heavner W, Pevny L. Eye Development and Retinogenesis. *Cold Spring Harbor Perspectives in Biology*. 2012;4(12):a008391-a008391. doi:10.1101/cshperspect.a008391

39. Heavner, W., & Pevny, L. (2012). Eye development and retinogenesis. Cold Spring Harbor perspectives in biology, 4(12), a008391. https://doi.org/10.1101/cshperspect.a008391

40. Holloway, E. M., Capeling, M. M., & Spence, J. R. (2019). Biologically inspired approaches to enhance human organoid complexity. *Development*, *146*(8), dev166173. https://doi.org/10.1242/dev.166173

41. Huang, E. J., Liu, W., Fritzsch, B., Bianchi, L. M., Reichardt, L. F., & Xiang, M. (2001). Brn3a is a transcriptional regulator of soma size, target field innervation and axon pathfinding of inner ear sensory neurons. Development (Cambridge, England), 128(13), 2421–2432.

42. Hufnagel RB, Le TT, Riesenberg AL, Brown NL. Neurog2 controls the leading edge of neurogenesis in the mammalian retina. *Developmental Biology*. 2010;340(2):490-503. doi:10.1016/j.ydbio.2010.02.002

43. Hunt, N. C., Hallam, D., Karimi, A., Mellough, C. B., Chen, J., Steel, D., & Lako, M. (2017). 3D culture of human pluripotent stem cells in RGD-alginate hydrogel improves retinal tissue development. Acta biomaterialia, 49, 329–343. https://doi.org/10.1016/j.actbio.2016.11.016

44. Isenmann S. Molecular determinants of retinal ganglion cell development, survival, and regeneration. *Progress in Retinal and Eye Research*. 2003;22(4):483-543. doi:10.1016/S1350-9462(03)00027-2

45. Jiang Y, Ding Q, Xie X, Libby RT, Lefebvre V, Gan L. Transcription Factors SOX4 and SOX11 Function Redundantly to Regulate the Development of Mouse Retinal Ganglion Cells. J Biol Chem. 2013;288(25):18429-18438. doi:10.1074/jbc.M113.478503

46. Kaya, K. D., Chen, H. Y., Brooks, M. J., Kelley, R. A., Shimada, H., Nagashima, K., de Val, N., Drinnan, C. T., Gieser, L., Kruczek, K., Erceg, S., Li, T., Lukovic, D., Adlakha, Y. K., Welby, E., & Swaroop, A. (2019). Transcriptome-based molecular staging of human stem cell-derived retinal organoids uncovers accelerated photoreceptor differentiation by 9-cis retinal. *Molecular vision*, *25*, 663–678.

47. Kim, J.-A., Kim, T.-W., Weinreb, R. N., Lee, E. J., Girard, M. J. A., & Mari, J. M. (2018). Lamina Cribrosa Morphology Predicts Progressive Retinal Nerve Fiber Layer Loss In Eyes with Suspected Glaucoma. *Scientific Reports*, *8*(1), 738. https://doi.org/10.1038/s41598-017-17843-8

48. Kim, S., Lowe, A., Dharmat, R., Lee, S., Owen, L. A., Wang, J., Shakoor, A., Li, Y., Morgan, D. J., Hejazi, A. A., Cvekl, A., DeAngelis, M. M., Zhou, Z. J., Chen, R., & Liu, W. (2019). Generation, transcriptome profiling, and functional validation of cone-rich human retinal organoids. Proceedings of the National Academy of Sciences of the United States of America, 116(22), 10824–10833. https://doi.org/10.1073/pnas.1901572116

49. Kolb H. Simple Anatomy of the Retina. 2005 May 1 [Updated 2012 Jan 31]. In: Kolb H, Fernandez E, Nelson R, editors. Webvision: The Organization of the Retina and Visual System [Internet]. Salt Lake City (UT): University of Utah Health Sciences Center; 1995-. Available from: https://www.ncbi.nlm.nih.gov/books/NBK11533/

50. Koulen, P., Fletcher, E. L., Craven, S. E., Bredt, D. S., & Wässle, H. (1998). Immunocytochemical localization of the postsynaptic density protein PSD-95 in the mammalian retina. *The Journal of neuroscience : the official journal of the Society for Neuroscience*, *18*(23), 10136–10149. https://doi.org/10.1523/JNEUROSCI.18-23-10136.1998

51. Komiya Y, Habas R. Wnt signal transduction pathways. *Organogenesis*. 2008;4(2):68-75. doi:10.4161/org.4.2.5851

52. Kurosu, H., Choi, M., Ogawa, Y., Dickson, A. S., Goetz, R., Eliseenkova, A. V., Mohammadi, M., Rosenblatt, K. P., Kliewer, S. A., & Kuro-O, M. (2007). Tissue-specific expression of betaKlotho and fibroblast growth factor (FGF) receptor isoforms determines metabolic activity of FGF19 and FGF21. The Journal of biological chemistry, 282(37), 26687–26695. https://doi.org/10.1074/jbc.M704165200

53. Kuwajima, T., Soares, C. A., Sitko, A. A., Lefebvre, V., & Mason, C. (2017). SoxC Transcription Factors Promote Contralateral Retinal Ganglion Cell Differentiation and Axon Guidance in the Mouse Visual System. Neuron, 93(5), 1110–1125.e5. https://doi.org/10.1016/j.neuron.2017.01.029

54. Laboissonniere, L.A., Goetz, J.J., Martin, G.M., Bi, R., Lund, T.J., Ellson, L., Lynch, M.R., Mooney, B., Wickham, H., Liu, P., Schwartz, G.W., & Trimarchi, J.M. Molecular signatures of retinal ganglion cells revealed through single cell profiling. Sci Rep 9, 15778 (2019). https://doi.org/10.1038/s41598-019-52215-4

55. Lakowski, J., Gonzalez-Cordero, A., West, E. L., Han, Y., Welby, E., Naeem, A., & Sowden, J. C. (2015). Transplantation of Photoreceptor Precursors Isolated via a Cell Surface Biomarker Panel from Embryonic Stem Cell-Derived Self-Forming Retina. *Stem Cells, 33*(8), 2469-2482. doi:10.1002/stem.2051

56. Lancaster, M. A., & Knoblich, J. A. (2014). Organogenesis in a dish: modeling development and disease using organoid technologies. Science (New York, N.Y.), 345(6194), 1247125. https://doi.org/10.1126/science.1247125

57. Lee, H. S., Bong, Y. S., Moore, K. B., Soria, K., Moody, S. A., & Daar, I. O. (2006). Dishevelled mediates ephrinB1 signalling in the eye field through the planar cell polarity pathway. Nature cell biology, 8(1), 55–63. https://doi.org/10.1038/ncb1344

58. Li, L., Knutsdottir, H., Hui, K., Weiss, M. J., He, J., Philosophe, B., Cameron, A. M., Wolfgang, C. L., Pawlik, T. M., Ghiaur, G., Ewald, A. J., Mezey, E., Bader, J. S., & Selaru, F. M. (2019). Human primary liver cancer organoids reveal intratumor and interpatient drug response heterogeneity. *JCI insight, 4*(2), e121490. Advance online publication. https://doi.org/10.1172/jci.insight.121490

59. Liu, Y., Wang, C., & Su, G. (2019). Cellular Signaling in Müller Glia: Progenitor Cells for Regenerative and Neuroprotective Responses in Pharmacological Models of Retinal Degeneration. Journal of ophthalmology, 2019, 5743109. https://doi.org/10.1155/2019/5743109

60. Llonch, S., Carido, M., & Ader, M. (2018). Organoid technology for retinal repair. *Developmental Biology*, *433*(2), 132–143. https://doi.org/10.1016/j.ydbio.2017.09.028

61. Luo Z, Xu C, Li K, Xian B, Liu Y, Li K, Liu Y, Rong H, Tang M, Hu D, Yang S, Ye M, Zhong X, Ge J. Islet1 and Brn3 Expression Pattern Study in Human Retina and hiPSC-Derived Retinal Organoid. *Stem Cells International*. 2019;2019:1-14. doi:10.1155/2019/8786396

62. Maddaluno L, Urwyler C, Werner S. Fibroblast growth factors: key players in regeneration and tissue repair. *Development*. 2017;144(22):4047-4060. doi:10.1242/dev.152587

63. Madelaine R, Mourrain P. Endogenous retinal neural stem cell reprogramming for neuronal regeneration. *Neural Regen Res*. 2017;12(11):1765. doi:10.4103/1673-5374.219028

64. Marques IJ, Lupi E, Mercader N. Model systems for regeneration: zebrafish. Development. 2019;146(18):dev167692. doi:10.1242/dev.167692

65. Masland R. H. (2012). The neuronal organization of the retina. Neuron, 76(2), 266–280.

66. Masri R. Neurons of the primate retina: A qualitative and quantitative analysis. Published online April 4, 2019. Accessed March 29, 2021. https://ses.library.usyd.edu.au/handle/2123/21165

67. Maurer-Stroh, S., Eisenhaber, B., & Eisenhaber, F. (2002). N-terminal N-myristoylation of proteins: refinement of the sequence motif and its taxon-specific differences. Journal of molecular biology, 317(4), 523–540. https://doi.org/10.1006/jmbi.2002.5425

68. Mazerik, J. N., Becker, S., & Sieving, P. A. (2018). 3-D retina organoids. *Cell Medicine*, *10*, 215517901877375. doi: 10.1177/2155179018773758

69. Mesentier-Louro, L. A., & Liao, Y. J. (2019). Optic Nerve Regeneration: Considerations on Treatment of Acute Optic Neuropathy and End-Stage Disease. *Current Ophthalmology Reports, 7*(1), 11-20. doi:10.1007/s40135-019-00194-0

70. Meyer, J. S., Howden, S. E., Wallace, K. A., Verhoeven, A. D., Wright, L. S., Capowski, E. E., & Gamm, D. M. (2011). Optic Vesicle-like Structures Derived from Human Pluripotent Stem Cells Facilitate a Customized Approach to Retinal Disease Treatment. *Stem Cells*, *29*(8), 1206–1218. doi: 10.1002/stem.674

71. Meyer, J. S., Shearer, R. L., Capowski, E. E., Wright, L. S., Wallace, K. A., Mcmillan, E. L., & Gamm, D. M. (2009). Modeling early retinal development with human embryonic and induce pluripotent stem cells. *Proceedings of the National Academy of Sciences*, *106*(39), 16698–16703. doi: 10.1073/pnas.0905245106

72. Nakano, T., Ando, S., Takata, N., Kawada, M., Muguruma, K., Sekiguchi, K., & Sasai, Y. (2012). Self-Formation of Optic Cups and Storable Stratified Neural Retina from Human ESCs. *Cell Stem Cell, 10*(6), 771-785. doi:10.1016/j.stem.2012.05.009

73. Nelson, R., Famiglietti, E. V., Jr, & Kolb, H. (1978). Intracellular staining reveals different levels of stratification for on- and off-center ganglion cells in cat retina. Journal of neurophysiology, 41(2), 472–483. https://doi.org/10.1152/jn.1978.41.2.472

74. Niewiadomski, P., Niedziółka, S. M., Markiewicz, Ł., Uśpieński, T., Baran, B., & Chojnowska, K. (2019). Gli Proteins: Regulation in Development and Cancer. Cells, 8(2), 147. https://doi.org/10.3390/cells8020147

75. Ort, V., & Howard, D. (n.d.). Development of the Eye. Retrieved April 10, 2021, from http://education.med.nyu.edu/courses/macrostructure/lectures/lec_images/eye.html#_Toc47350009

76. Pan, L., Yang, Z., Feng, L., & Gan, L. (2005). Functional equivalence of Brn3 POU-domain transcription factors in mouse retinal neurogenesis. Development (Cambridge, England), 132(4), 703–712. https://doi.org/10.1242/dev.01646

77. Perrimon, N., Pitsouli, C., & Shilo, B. Z. (2012). Signaling mechanisms controlling cell fate and embryonic patterning. Cold Spring Harbor perspectives in biology, 4(8), a005975. https://doi.org/10.1101/cshperspect.a005975

78. Prasad, T. K., & Rao, N. M. (2005). The role of plasmid constructs containing the SV40 DNA nuclear-targeting sequence in cationic lipid-mediated DNA delivery. Cellular & molecular biology letters, 10(2), 203–215.

79. Provis, J. M., van Driel, D., Billson, F. A., & Russell, P. (1985). Development of the human retina: patterns of cell distribution and redistribution in the ganglion cell layer. The Journal of comparative neurology, 233(4), 429–451. https://doi.org/10.1002/cne.902330403

80. Qian, X., Song, H., & Ming, G. (2019). Brain organoids: advances, applications and challenges. *Development*, *146*(8), dev166074. https://doi.org/10.1242/dev.166074

81. Ramachandran, R., Fausett, B. V., & Goldman, D. (2010). Ascl1a regulates Müller glia dedifferentiation and retinal regeneration through a Lin-28-dependent, let-7 microRNA signalling pathway. Nature cell biology, 12(11), 1101–1107. https://doi.org/10.1038/ncb2115

82. Rueda EM, Hall BM, Hill MC, Swinton PG, Tong X, Martin JF, Poché RA. The Hippo Pathway Blocks Mammalian Retinal Müller Glial Cell Reprogramming. *Cell Reports*. 2019;27(6):1637-1649.e6. doi:10.1016/j.celrep.2019.04.047

83. Sanes, J. R., & Masland, R. H. (2015). The types of retinal ganglion cells: Current status and implications for neuronal classification. *Annual Review of Neuroscience, 38*(1), 221-246. doi:10.1146/annurev-neuro-071714-034120

84. Schiller PH, Sandell JH, Maunsell JHR. Functions of the ON and OFF channels of the visual system. *Nature*. 1986;322(6082):824-825. doi:10.1038/322824a0

85. Schnapp E. Hedgehog signaling controls dorsoventral patterning, blastema cell proliferation and cartilage induction during axolotl tail regeneration. *Development*. 2005;132(14):3243-3253. doi:10.1242/dev.01906

86. Singh, R., Cuzzani, O., Binette, F., Sternberg, H., West, M. D., & Nasonkin, I. O. (2018). Pluripotent Stem Cells for Retinal Tissue Engineering: Current Status and Future Prospects. Stem cell reviews and reports, 14(4), 463–483. https://doi.org/10.1007/s12015-018-9802-4

87. Singhal, S., Bhatia, B., Jayaram, H., Becker, S., Jones, M. F., Cottrill, P. B., Khaw, P. T., Salt, T. E., & Limb, G. A. (2012). Human Müller glia with stem cell characteristics differentiate into retinal ganglion cell (RGC) precursors in vitro and partially restore RGC function in vivo following transplantation. Stem cells translational medicine, 1(3), 188–199. https://doi.org/10.5966/sctm.2011-0005

88. Spira, A. W., & Hollenberg, M. J. (1973). Human retinal development: ultrastructure of the inner retinal layers. Developmental biology, 31(1), 1–21.

89. Stefan, C., Batras, M., Iliescu Daniela, A., Timaru Cristina, M., De Simone, A., & Hosseini-Ramhormozi, J. (2015). CURRENT OPTIONS FOR SURGICAL TREATMENT OF GLAUCOMA. *Romanian journal of ophthalmology*, *59*(3), 194–201.

90. Tamm, E. R., & Ohlmann, A. (2012). Entwicklung des menschlichen Auges [Development of the human eye]. Der Ophthalmologe : Zeitschrift der Deutschen Ophthalmologischen Gesellschaft, 109(9), 911–928. https://doi.org/10.1007/s00347-012-2644-6

91. Tamm, E., Ohlmann, A. Development of the human eye. Ophthalmologist 109 : 911-928 (2012).

92. Tang, Y., Jackson, M., Qian, K., & Phillips, M. I. (2002). Hypoxia inducible double plasmid system for myocardial ischemia gene therapy. Hypertension (Dallas, Tex. : 1979), 39(2 Pt 2), 695–698. https://doi.org/10.1161/hy0202.103784

93. Vaithianathan, T., Akmentin, W., Henry, D., & Matthews, G. (2013). The ribbon-associated protein C-terminal-binding protein 1 is not essential for the structure and function of retinal ribbon synapses. *Molecular vision*, *19*, 917–926.

94. Vergara MN, Del Rio-Tsonis K. Retinal regeneration in the Xenopus laevis tadpole: a new model system. *Mol Vis*. 2009;15:1000-1013.

95. Völkner, M., Zschätzsch, M., Rostovskaya, M., Overall, R. W., Busskamp, V., Anastassiadis, K., & Karl, M. O. (2016). Retinal Organoids from Pluripotent Stem Cells Efficiently Recapitulate Retinogenesis. Stem cell reports, 6(4), 525–538. https://doi.org/10.1016/j.stemcr.2016.03.001

96. Wahlin, K.J., Maruotti, J.A., Sripathi, S.R., Ball, J., Angueyra, J.M., Kim, C., Grebe, R., Li, W., Jones, B.W., & Zack, D.J. Photoreceptor Outer Segment-like Structures in Long-Term 3D Retinas from Human Pluripotent Stem Cells. *Sci Rep* **7,** 766 (2017). https://doi.org/10.1038/s41598-017-00774-9

97. Walker, A., Su, H., Conti, M. A., Harb, N., Adelstein, R. S., & Sato, N. (2010). Non-muscle myosin II regulates survival threshold of pluripotent stem cells. *Nature communications*, *1*, 71. https://doi.org/10.1038/ncomms1074

98. Wan J, Goldman D. Retina regeneration in zebrafish. *Current Opinion in Genetics & Development*. 2016;40:41-47. doi:10.1016/j.gde.2016.05.009

99. Wang RN, Green J, Wang Z, Deng Y, Qiao M, Peabody M, Zhang Q, Ye J, Yan Z, Denduluri S, Idowu O, Li M, Shen C, Hu A, Haydon RC, Kang R, Mok J, Lee MJ, Luu HL, Shi LL. Bone Morphogenetic Protein (BMP) signaling in development and human diseases. *Genes & Diseases*. 2014;1(1):87-105. doi:10.1016/j.gendis.2014.07.005

100. Wang Y, Yu A, Yu F-X. The Hippo pathway in tissue homeostasis and regeneration. *Protein Cell*. 2017;8(5):349-359. doi:10.1007/s13238-017-0371-0

101. Wang, C., Ward, M. E., Chen, R., Liu, K., Tracy, T. E., Chen, X., Xie, M., Sohn, P. D., Ludwig, C., Meyer-Franke, A., Karch, C. M., Ding, S., & Gan, L. (2017). Scalable Production of iPSC-Derived Human Neurons to Identify Tau-Lowering Compounds by High-Content Screening. Stem cell reports, 9(4), 1221–1233. https://doi.org/10.1016/j.stemcr.2017.08.019

102. Wang, Q., Marcucci, F., Cerullo, I., & Mason, C. (2016). Ipsilateral and Contralateral Retinal Ganglion Cells Express Distinct Genes during Decussation at the Optic Chiasm. eNeuro, 3(6), ENEURO.0169-16.2016. https://doi.org/10.1523/ENEURO.0169-16.2016

103. Weinreb, R. N., Aung, T., & Medeiros, F. A. (2014). The pathophysiology and treatment of glaucoma: a review. JAMA, 311(18), 1901–1911. https://doi.org/10.1001/jama.2014.3192

104. Whyte JL, Smith AA, Helms JA. Wnt Signaling and Injury Repair. *Cold Spring Harbor Perspectives in Biology*. 2012;4(8):a008078-a008078. doi:10.1101/cshperspect.a008078

105. Wu F, Kaczynski TJ, Sethuramanujam S, Li R, Jain V, Slaughter M, Mu X. Two transcription factors, Pou4f2 and Isl1, are sufficient to specify the retinal ganglion cell fate. *Proc Natl Acad Sci USA*. 2015;112(13):E1559-E1568. doi:10.1073/pnas.1421535112

106. Xia H, Li X, Gao W, Fu X, Fang RH, Zhang L, Zhang K. Tissue repair and regeneration with endogenous stem cells. Nat Rev Mater. 2018;3(7):174-193. doi:10.1038/s41578-018-0027-6

107. Xu, Y., Zhu, X., Hahm, H. S., Wei, W., Hao, E., Hayek, A., & Ding, S. (2010). Revealing a core signaling regulatory mechanism for pluripotent stem cell survival and self-renewal by small molecules. *Proceedings of the National Academy of Sciences of the United States of America*, *107*(18), 8129–8134. https://doi.org/10.1073/pnas.1002024107

108. Xiang M, Jiang H, Jin K, Qiu F. Molecular Control of Retinal Ganglion Cell Specification and Differentiation. In: Rumelt S, ed. *Glaucoma - Basic and Clinical Concepts*. InTech; 2011. doi:10.5772/19832

109. Xiao D, Qiu S, Huang X, Zhang R, Lei Q, Huang W, Chen H, Gou B, Tie X, Liu S, Liu Y, Jin K, Xiang M. *Directed Robust Generation of Functional Retinal Ganglion Cells from Müller Glia*. Neuroscience; 2019. doi:10.1101/735357

110. Yu L, Han M, Yan M, Lee E-C, Lee J, Muneoka K. BMP signaling induces digit regeneration in neonatal mice. *Development*. 2010;137(4):551-559. doi:10.1242/dev.042424

111. Zaghloul, N. A., Yan, B., & Moody, S. A. (2005). Step-wise specification of retinal stem cells during normal embryogenesis. Biology of the cell, 97(5), 321–337. https://doi.org/10.1042/BC20040521

112. Zhang, XM., Hashimoto, T., Tang, R., & Yang, X.J. (2018). Elevated expression of human bHLH factor ATOH7 accelerates cell cycle progression of progenitors and enhances production of avian retinal ganglion cells. Sci Rep 8, 6823. https://doi.org/10.1038/s41598-018-25188-z

113. Zhong, X., Gutierrez, C., Xue, T., Hampton, C., Vergara, M. N., Cao, L.-H., Canto-Soler, M. V. (2014). Generation of three-dimensional retinal tissue with functional photoreceptors from human iPSCs. *Nature Communications*, *5*(1). doi: 10.1038/ncomms5047

114. Zuber, M. E., Gestri, G., Viczian, A. S., Barsacchi, G., & Harris, W. A. (2003). Specification of the vertebrate eye by a network of eye field transcription factors. Development (Cambridge, England), 130(21), 5155–5167. https://doi.org/10.1242/dev.00723